Colossal dielectric constants in transition-metal oxides

P. Lunkenheimer[1,a], S. Krohns[1], S. Riegg[2], S.G. Ebbinghaus[3], A. Reller[2], and A. Loidl[1]

[1] Experimental Physics V, Center for Electronic Correlations and Magnetism, University of Augsburg, 86135 Augsburg, Germany
[2] Solid State Chemistry, University of Augsburg, 86135 Augsburg, Germany
[3] Solid State Chemistry, Martin-Luther University Halle-Wittenberg, 06120 Halle, Germany

Abstract. Many transition-metal oxides show very large ("colossal") magnitudes of the dielectric constant and thus have immense potential for applications in modern microelectronics and for the development of new capacitance-based energy-storage devices. In the present work, we thoroughly discuss the mechanisms that can lead to colossal values of the dielectric constant, especially emphasising effects generated by external and internal interfaces, including electronic phase separation. In addition, we provide a detailed overview and discussion of the dielectric properties of $CaCu_3Ti_4O_{12}$ and related systems, which is today's most investigated material with colossal dielectric constant. Also a variety of further transition-metal oxides with large dielectric constants are treated in detail, among them the system $La_{2-x}Sr_xNiO_4$ where electronic phase separation may play a role in the generation of a colossal dielectric constant.

1 Introduction

Hot topics like high-T_c superconductivity, colossal magnetoresistance and multiferroicity have led to a tremendous boost of solid state physics during the last 25 years. These and other interesting phenomena to a large extend first have been revealed and intensely investigated in transition-metal oxides. The complexity of the ground states of these materials arises from strong electronic correlations, enhanced by the interplay of spin, orbital, charge and lattice degrees of freedom. These phenomena are a challenge for basic research and also bear enormous potentials for future applications as the related ground states are often accompanied by so-called "colossal" effects, which are possible building blocks for tomorrows correlated electronics.

The measurement of the response of transition-metal oxides to ac electric fields is one of the most powerful techniques to provide detailed insight into the underlying physics that may comprise very different phenomena, e.g., charge order, molecular or polaronic relaxations, magnetocapacitance, hopping charge transport, ferroelectricity or density-wave formation. The present work concentrates on materials showing so-called colossal dielectric constants (CDC), i.e. values of the real part of the permittivity ε' exceeding 1000. Since long, materials with high dielectric constants are in the focus of interest, not only for purely academic reasons but also because new high-ε' materials are urgently sought after for the further development of modern electronics. In general, for the miniaturisation of capacitive electronic elements materials with high-ε' are prerequisite. This is true not only for the common silicon-based integrated-circuit technique but also for stand-alone capacitors. For example, the latter, if constructed using materials with CDCs, can reach capacitances high enough to enable their use for energy storage,

[a] e-mail: peter.lunkenheimer@physik.uni-augsburg.de

without the disadvantage of escalating volume and weight. Such capacitors can be used, e.g., to replace batteries in hybrid vehicles.

Most of the currently available capacitor materials with CDCs are based on ferroelectrics, which reach very high values of the dielectric constant often exceeding 10^4. However, ferroelectric materials exhibit a strong temperature dependence of ε', limiting their straightforward application in electronic devices. Currently, the most prominent non-ferroelectric material showing colossal values of ε' is $CaCu_3Ti_4O_{12}$ (CCTO). Initiated by the first reports of extremely high dielectric constants in CCTO in 2000 [1] and further boosted by the article of Homes *et al.* [2] appearing in "Science" in the following year, until now more than 380 papers have been published on this and related materials. The fact that among them there are more than ten so-called "highly-cited" papers [3] (e.g., [1,2,4,5,6,7,8,9,10,11,12,13,14]) demonstrates the tremendous interest in new high-ε' materials. The big advantage of CCTO compared to ferroelectric-based dielectrics is its nearly temperature independent CDC around room temperature. Only below about 200 K (depending on frequency) it shows a marked and strongly frequency-dependent decrease of $\varepsilon'(T)$ from values up to 10^5 to magnitudes of the order of 100. Many speculations about the origin of the CDCs in CCTO have been put forward. Already in the original work by Subramanian *et al.* [1] a barrier layer mechanism [10,15,16,17,18] was suggested, arising from twin boundaries. However, in some other early works intrinsic bulk mechanisms were proposed for the explanation of the CDCs in CCTO. This includes relaxational excitations of highly polarizable entities of unspecified origin [4], geometrically frustrated ferroelectric order caused by symmetrical off-centre displacements of Ti ions [2] and a special kind of defects in the perovskite structures relaxing between different equivalent configurations [19]. After the thorough investigation of this material in numerous works during the last ten years, nowadays it is quite commonly accepted that a barrier mechanism is the correct explanation (see, e.g., [5,8,9,10,11,12,20,21,22,23]). However, the nature of these barriers leading to the CDCs in CCTO still is an open question. There are various reports on experimental results that seem to support internal [5,8,9,12,20,21,22,23] or surface barrier layer capacitors [11,24,25,26,27] (IBLCs or SBLCs, respectively) giving rise to the detected CDCs. The first could stem from grain boundaries (in ceramic samples) and/or from boundaries between twins (or other planar defects) within single crystals or within the crystallites of ceramic samples. SBLCs may arise from the depletion layers of Schottky or metal-insulator-semiconductor (MIS) diodes at the interfaces between the metallic electrodes and the bulk sample.

Despite huge efforts, the properties of CCTO seem to be not ideal for straightforward application if considering the amplitude of its dielectric loss, the downscaling of its properties to miniaturised devices and its applicability at frequencies in the increasingly important frequency range around GHz [11,26]. Thus there is still an ongoing search for new, better materials. There is a vast number of materials isostructural to CCTO, which may also show CDCs but have only partly been characterised so far [1,6,28,29,30,31]. But also completely different transition-metal oxides have been reported to exhibit CDCs and it seems that this phenomenon is quite common in this class of materials (e.g., [10,32,33,34,35,36,37,38,39,40,41,42,43,44,45,46,47,48,49,50,51,52]). In addition other mechanisms for the generation of CDCs are considered. For example, the formation of CDCs by internal interfaces spontaneously arising via electronic phase separation (e.g., stripe-ordering) seems one of the most feasible ways to accomplish materials that are suitable for application.

In the following we will give an overview of the different ways of generating CDCs, laying special emphasis on interface-related mechanisms. Then we will provide and discuss various results on CCTO, CCTO-related materials and other transition-metal oxides with CDCs.

2 Mechanisms giving rise to colossal dielectric constants

The most prominent mechanisms that can give rise to enhanced values of the dielectric constant are ferroelectricity, charge-density wave formation, hopping charge transport, the metal-insulator transition and various kinds of interface effects. In a first step we would like to get a rough guess about the maximum dielectric constant that can be reached in ionic solids without

permanent dipole moments and without invoking any of these mechanisms. The static dielectric constant ε_s in an ionic solid is given by $\varepsilon_s = \varepsilon_\infty + (\Omega_p/\omega_T)^2$. Here ε_∞ is the electronic dielectric constant determined at frequencies beyond the phonon modes, Ω_p is the effective ionic plasma frequency and ω_T the eigenfrequency of a transverse optical vibration, which can be directly observed in infrared experiments. The ionic plasma frequency is given by $\Omega_p^2 = \varepsilon_\infty N(Ze)^2/(V\varepsilon_0\mu)$, where N is the number of ionic pairs of effective charge Ze per volume V, ε_0 is the vacuum dielectric permittivity and μ the reduced mass of the ion pair involved in the eigenmode. Large dielectric constants demand large ionic plasma frequencies and small eigenfrequencies of the infrared active mode. Large plasma frequencies are reached via large effective charges and low masses. It is clear that in the oscillator model small masses and small eigenfrequencies are related via $\omega \propto 1/\sqrt{\mu}$ and can hardly be reached at the same time if soft-mode scenarios are not taken into consideration. To get some estimate of the largest possible value of the dielectric constant we make the following assumptions: $\varepsilon_\infty = 10$, $Z = 3$, $N = 1$ per unit cell volume $V = 64$ Å^3 and $\mu = 12$ in units of the atomic mass constant. These numbers can be reached assuming an ion pair with Ti^{4+} vibrating against O^{2-} and yield an effective ionic plasma frequency $\Omega_p/2\pi \approx 72$ THz. The resulting dielectric constant now depends significantly on the eigenfrequency of the mode under consideration. Assuming $\omega_T/2\pi = 2.3$ THz yields $\varepsilon_s \approx 1000$; taking an eigenfrequency which better correlates with the low reduced masses, namely $\omega_T/2\pi = 7$ THz, results in a dielectric constant $\varepsilon_s \approx 120$, which comes close to the maximum value of experimentally observed dielectric constants in purely ionic solids. Thus for the generation of CDCs, other mechanisms have to be considered as discussed in the following.

2.1 Ferroelectricity

It is known since long that in ferroelectrics very high values of the dielectric constant can arise [53,54]. Approaching the ferroelectric phase transition at T_c from high temperatures, $\varepsilon'(T)$ strongly increases, usually following a Curie-Weiss behaviour and starts to decrease again below T_c. In addition, ferroelectrics have pronounced non-linear dielectric properties, e.g., showing characteristic hysteresis loops of the electric-field dependent polarisation [54]. Both phenomena represent problems for application in electronic devices. This partly can be overcome by doping and special processing thereby adjusting microstructure and internal interfaces. The well-known ceramic Barrier Layer Capacitors use a combination of interface polarisation effects and ferroelectric materials like $BaTiO_3$ to achieve high capacitance values with temperature and voltage dependences that are tolerable at least for some applications [55,56,57]. Ferroelectric transitions often are classified as displacive or order-disorder type. The latter case corresponds to the ordering of dipolar degrees of freedom already present at $T > T_c$. In these systems the hopping of the dipoles can lead to strong frequency dependence of ε' at technically relevant frequencies (Hz-GHz) making them less suited for application [54,58,59]. In contrast, ferroelectrics of displacive type usually show no frequency dependence up to infrared frequencies, where the well-known soft-phonon modes appear [54].

A special variant of ferroelectrics are the so-called relaxor ferroelectrics [60,61]. Their static dielectric constant shows a strong increase with decreasing temperature just as for canonical ferroelectrics. However, this is superimposed by a marked relaxation mode that leads to peaks in $\varepsilon'(T)$ at temperatures that are strongly dependent on frequency. Different explanations have been proposed for this behaviour, e.g., in terms of polar cluster dynamics, but no consensus has been achieved so far [60,61,62,63,64].

While in conventional and relaxor ferroelectrics ions or dipoles are the relevant entities achieving ferroelectric order, also the ordering of electronic degrees of freedom has been considered [42,65,66,67]. For example, the occurrence of CDCs of magnitude > 4000 detected in the mixed-valent transition-metal oxide $LuFe_2O_4$ was ascribed to an electronic polarisation mechanism involving charge ordering of Fe^{2+} and Fe^{3+} ions [42]. Also in certain charge-transfer salts a ferroelectric transition of electronic origin recently was discussed [58,68].

Finally, it should be mentioned that in some materials, the so-called incipient ferroelectrics, long-range ferroelectric order is prevented by quantum fluctuations at low temperature, setting in before complete order is achieved at T_c. At temperatures sufficiently above T_c, $\varepsilon'(T)$

of these materials follows the Curie-Weiss law and thus CDCs are observed. The most prominent incipient ferroelectric is $SrTiO_3$ [69], which shows a tendency of $\varepsilon'(T)$ to saturate at low temperatures, setting in below about 30 K due to the mentioned quantum effects [70]. Besides $BaTiO_3$, also $SrTiO_3$ is often employed as dielectric material in commercial ceramic Barrier Layer Capacitors.

2.2 Charge-Density Waves

In highly anisotropic low-dimensional materials a metal-insulator transition can arise with lowering of the temperature, which is accompanied by the formation of a charge-density wave (CDW). Here the electronic charge density is a periodic function of position and its period can be incommensurate with the crystal lattice. A very well-known example of a CDW system is also found in the group of transition-metal oxides, namely the blue bronze, $K_{0.30}MoO_3$ [71]. The dielectric behaviour of CDW systems shows two characteristic features: A harmonic oscillator mode at GHz frequencies caused by the CDW being pinned at defects and a huge relaxation mode at kHz-MHz involving colossal values of the dielectric constant [72,73,74]. In CDW systems the highest intrinsic dielectric constants of any materials are observed, reaching magnitudes of up to 10^8. Littlewood [75] has proposed screening effects of the pinned CDW by the normal electrons, not participating in the CDW, to explain the occurrence of the low-frequency relaxation mode and CDCs in this class of materials. Due to the strong frequency dependence of ε' and the high dielectric losses associated with the relaxational modes, CDWs are not applied in capacitive devices.

2.3 Hopping charge transport

Hopping conductivity is the most common charge-transport process in condensed matter. As it is intimately related with the occurrence of a power law with negative exponent in the frequency-dependent dielectric constant $\varepsilon'(\nu)$, it will always lead to a divergence of ε' for low frequencies [76,77,78,79]. Hopping conduction is the typical charge-transport process of localised charge carriers. In electronic conductors, electrons (or holes) can localise due to disorder. Disorder may arise from an amorphous structure, from doping (substitutional disorder) or occur even in nominally pure crystals due to slight deviations from stoichiometry or lattice imperfections. Hopping conduction leads to a characteristic signature in the frequency dependence of the complex conductivity, namely a power-law increase $\sigma' = \sigma_0\nu^s$ with the exponent $s < 1$ [76,77,80]. This power law was shown by Jonscher [78,79] to be a quite universal phenomenon in all types of disordered matter and termed "Universal Dielectric Response" (UDR). This behaviour can be understood in the framework of various models on the charge transport of localised charge carriers, including the often-employed variable-range hopping (VRH) model [76,77,80]. These models originally were developed for amorphous and highly doped semiconductors like doped silicon but also, e.g., for thin scandium-oxide films [76,77,80,81,82]. The typical signature of hopping transport in measurements of the ac conductivity was also found in numerous transition-metal oxides (e.g., [11,26,44,45,46,48,49,50,51,82,83,84,85]). Via the Kramers-Kronig relation, the ν^s power law also leads to a corresponding power law in the imaginary part of the ac conductivity, namely $\sigma'' = \tan(s\pi/2)\sigma_0\nu^s$ [79]. As the dielectric constant is directly related to σ'' via $\varepsilon' = \sigma''/(2\pi\nu\varepsilon_0)$ (with ε_0 the permittivity of vacuum) hopping conduction is expected to lead to a power law $\varepsilon' \propto \nu^{s-1}$. Thus, as $s < 1$, the dielectric constant can easily reach colossal magnitudes for low frequencies. However, as the factor $tan(s\pi/2)$ usually is of the order of one, the dielectric loss $\varepsilon'' = \sigma'/(2\pi\nu\varepsilon_0)$ is relatively high (which of course is reasonable for a conducting material) rendering this effect unsuited for application.

2.4 Metal-insulator transition

It is known since about 100 years that the Clausius-Mosotti relation will lead to a polarisation catastrophe, i.e. a divergence of the dielectric constant when approaching the metal-insulator

(MI) transition from the insulating side [86]. It is naively clear that the reduction of the restoring forces experienced by electrons localised at atomic sites, which should occur when the material approaches the metallic state with its itinerant electron states, will lead to an increase of the electronic polarisability and thus the dielectric constant. Indeed, such a divergence has been observed in some cases [86,87,88,89,90], the most prominent one being measurements of the dielectric properties of doped silicon for increasing doping level [88]. Several theoretical approaches have appeared treating this topic and going beyond the simple arguments based on the Clausius-Mosotti equation [91,92,93,94]. Prototypical MI transitions are regularly found in transition-metal oxides, the most well-known ones being those in magnetite, Fe_3O_4, and vanadium oxide, V_2O_3. One may speculate if some of the observations of CDCs in transition-metal oxides [10,32,33,34,35,36,37,38,39,40,41,42,43,44,45,46,47,48,49,50,51,90] could be due to the fact that these materials often are at the verge of a MI transition. However, in most cases interfacial effects as treated in the following section seem the more likely explanation. The expected divergence of ε' at the MI transition of course is also accompanied by an increase of the conductivity, preventing any technical application of this effect for the construction of capacitive components.

2.5 Interface effects

Interfaces of any kind can generate very high apparent values of the dielectric constant because they act as parallel-plate capacitors with very small plate distances, thus having high capacitances [10]. This corresponds to the long-known Maxwell-Wagner (MW) polarisation effects. Originally, Maxwell and Wagner developed their models for three different types of heterogeneous samples, namely for a dielectric sample consisting of layers with different dielectric properties (i.e. ε' and σ') arranged perpendicular to the electric field, for an ideal dielectric sample covered with a bad conductor of varying thickness and for a homogeneous dielectric medium in which spherical particles with different dielectric properties are suspended [15,16]. For all these cases, strong dispersion of the dielectric constant and of the loss was deduced, which can be completely understood from the heterogeneity of the investigated samples without invoking any frequency-dependent microscopic processes within the dielectric materials.

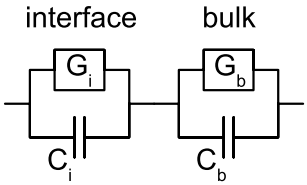

Fig. 1. Equivalent circuit representing the simplest model for a heterogeneous sample, composed, e.g., of an interfacial and bulk region.

A straightforward approach to understand the dielectric behaviour of such a heterogeneous system is an equivalent circuit analysis [18,79]. Let us assume the simplest case of the sample being composed of two regions with different dielectric properties. Each region, of course, has some conductivity and dielectric constant, i.e. represents a lossy capacitor. It shall be modeled by a simple parallel RC circuit, i.e. we assume that there is no intrinsic frequency dependence of conductivity or dielectric constant. For the cases treated by Maxwell and Wagner [15,16] and for any cases where the second dielectric region is of interfacial type as, e.g., a grain boundary or a surface depletion layer, it seems reasonable to assume a serial connection of the two RC circuits as depicted in Fig. 1. Then the total admittance of this circuit is given by $Y_t = G'_t + iG''_t = (G_i + i\omega C_i)(G_b + i\omega C_b)/[(G_i + i\omega C_i) + (G_b + i\omega C_b)]$ ($\omega = 2\pi\nu$ is the circular

frequency). When resolved into real and imaginary part and calculating the capacitances via $C'_t = G''/\omega$ and $C''_t = G'/\omega$, we obtain:

$$C''_t = \frac{G_i G_b (G_i + G_b) + \omega^2 (G_i C_b^2 + G_b C_i^2)}{\omega (G_i + G_b)^2 + \omega^3 (C_i + C_b)^2} \tag{1}$$

$$C'_t = \frac{(G_i^2 C_b + G_b^2 C_i) + \omega^2 C_i C_b (C_i + C_b)}{(G_i + G_b)^2 + \omega^2 (C_i + C_b)^2} \tag{2}$$

Here G_b and G_i are the conductances and C_b and C_i are the capacitances of the different sample regions with indices b and i standing for bulk and interface, respectively. If neglecting the geometry factors connecting C and ε', these relations lead to exactly the same frequency dependence as the Debye relaxation laws,

$$\varepsilon' = \varepsilon_\infty + \frac{\varepsilon_s - \varepsilon_\infty}{1 + \omega^2 \tau^2} \tag{3}$$

and

$$\varepsilon'' = \frac{(\varepsilon_s - \varepsilon_\infty)\omega\tau}{1 + \omega^2 \tau^2} + \frac{\sigma_{dc}}{\omega \varepsilon_0}, \tag{4}$$

describing the relaxational response of an ideal dipolar system (Fig. 2) [95]. Here ε_s and ε_∞ are the low and high frequency limits of $\varepsilon'(\omega)$, respectively, and τ is the relaxation time, describing the dipolar dynamics. The last term in Eq. (4) accounts for the contribution of dc charge transport to the loss, with σ_{dc} the dc conductivity. The quantities of Eqs. 1 and 2 corresponding to ε_s, ε_∞ and τ are:

$$C'_s = \frac{G_i^2 C_b + G_b^2 C_i}{(G_i + G_b)^2} \tag{5}$$

$$C'_\infty = \frac{C_i C_b}{C_i + C_b} \tag{6}$$

$$\tau = \frac{C_i + C_b}{G_i + G_b} \tag{7}$$

Nowadays any relaxational response generated by heterogeneities in the sample is termed MW relaxation.

Let us now assume that one of the two dielectric regions of the sample indeed is an insulating interface like the depletion layer of a Schottky diode at the electrodes or like barrier layers between the grains of a polycrystalline sample. In the latter case we make the simplifying assumption that all grain boundaries act like a single capacitor, which is justified in most cases (there are more detailed treatments like the brick layer model [18,96,97] but they lead to essentially the same results). Then we can assume that $C_i \gg C_b$ (the interface is much thinner than the bulk) and that $G_i \ll G_b$ (the interface is nearly insulating). In this limit we get $C'_s = C_i$, $C'_\infty = C_b$ and $\tau = C_i/G_b$. Thus at low frequencies, the dielectric constant is completely governed by the large capacitance of the thin insulating interface layer and only at high frequencies the intrinsic bulk response is detected (by the way, the same goes for the conductance, i.e. $G'_t(\nu \to 0) = G_i$ and $G'_t(\nu \to \infty) = G_b$). This can be rationalised by the bridging of the high contact resistance by the contact capacitance, acting like a short at high frequencies [10]. When evaluating dielectric measurements, the dielectric constant usually is calculated from the measured capacitance data via $\varepsilon' = C'/C_0$. C_0 is the geometrical capacitance, for a parallel-plate capacitor given by $C_0 = \varepsilon_0 A/t$ with A the area and t the plate distance of the capacitor. At low frequencies, in the interface dominated regime, of course C_0 determined from the bulk geometry is the wrong quantity and can be many decades smaller than the geometrical capacitance of the thin insulating layer(s). Thus, despite the true dielectric constant of the interface region (and of course that of the bulk) have "normal" magnitudes, say of the order of ten, very large apparent values of ε' can arise [10]. It is difficult to distinguish these effects

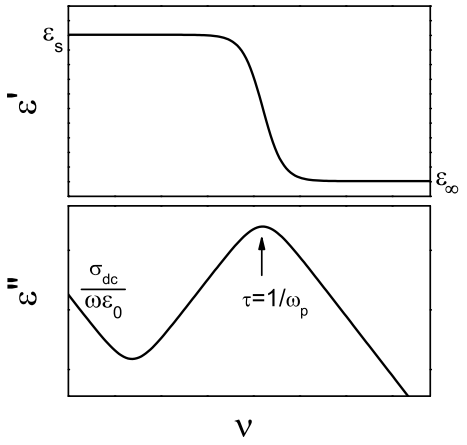

Fig. 2. Dielectric response for a Debye relaxation arising from the polarisation of dipolar degrees of freedom with an additional contribution from dc charge transport. In the loss a peak arises in $\omega_p = 1/\tau$. Identical spectra are also produced by the equivalent circuit shown in Fig. 1 without invoking any intrinsic frequency dependence of the circuit elements.

from true bulk contributions as the resulting relaxation modes have all the characteristics of intrinsic relaxations, where dipolar entities are assumed to reorient in accord with the ac field at low frequencies but to be unable to follow its quick variations at high frequency. Also the typical frequency-dependent shifts of the relaxation features, mirroring in the intrinsic case the freezing of dipolar dynamics at low temperatures [95], are observed: The bulk conductance G_b of the considered materials usually has semiconducting temperature characteristics, i.e. it increases exponentially with temperature. Thus, via the relation $\tau = C_i/G_b$ the relaxation time will exhibit the typical strong temperature variation of dipolar systems leading to pronounced shifts of the step in $\varepsilon'(\nu)$ and the peak in $\varepsilon''(\nu)$ to low frequencies when temperature is reduced, just as for an intrinsic dipolar relaxation.

Real-life samples exhibiting interfacial polarisation usually do not exactly follow the behaviour suggested by Eqs. 1 and 2 and depicted in Fig. 2. For example, the step in $\varepsilon'(\nu)$ and the peak in $\varepsilon''(\nu)$ sometimes are smeared out and significantly broader than expected. Just as for systems showing intrinsic dipolar relaxations [98,99], this can be ascribed to a distribution of relaxation times. For heterogeneity-generated MW relaxations it can be assumed to arise, e.g., from the roughness of the surface in case of a Schottky-diode mechanism or from the distribution of grain (and thus also grain-boundary) sizes in ceramic samples. In addition, the ubiquitous hopping conductivity usually leads to the typical power-law frequency dependences of the UDR [79], i.e. $\sigma' \propto \nu^s$, $\sigma'' \propto \nu^s$, $\varepsilon' \propto \nu^{s-1}$ and $\varepsilon'' \propto \nu^{s-1}$ with $s < 1$ (see Sec. 2.3), which determines the spectra in the high-frequency regime where the intrinsic bulk behaviour governs the dielectric response. The resulting curves are schematically shown in Fig. 3 (solid lines) [10]. The dashed lines represent the pure intrinsic behaviour of the bulk sample, which would be observed in the absence of any interface contributions. Finally, in heterogeneity dominated samples often an additional relaxation leading to even higher values of ε' at the lowest frequencies is found as schematically illustrated by the dotted lines in Fig. 3. This implies the presence of two different interfacial regions in the sample, which can be rationalised, e.g., by the simultaneous presence of a surface depletion layer and insulating grain or twinning boundaries [11,26,27]. Thus, the most general equivalent circuit is provided by two parallel RC circuits, connected in series to the bulk element, the latter consisting of a capacitance, dc resistor and a frequency-dependent complex conductance element accounting for the hopping-generated UDR (inset of Fig. 3(c)).

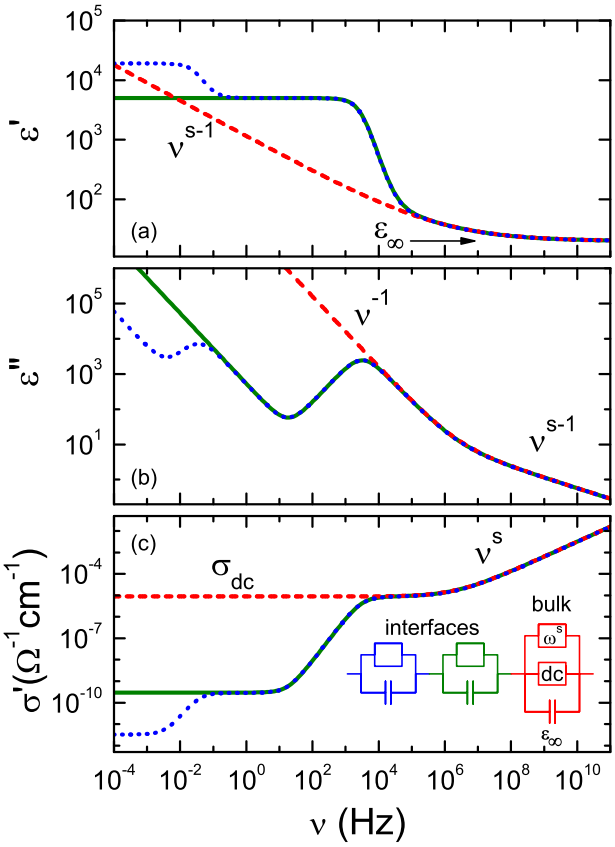

Fig. 3. Frequency-dependent dielectric response for the equivalent circuit shown in (c). Dashed lines: Intrinsic bulk response. Solid and dotted lines: Overall response with one, respectively two additional RC-circuits. The circuit parameters have been chosen to reveal the prototypical behaviour of doped semiconductors with Schottky-barrier-type contacts [10].

As mentioned above, insulating interfaces can occur at the surface of the sample, e.g., due to the formation of a Schottky diode at the electrode/sample contact or due to a thin insulating surface layer with slightly different stoichiometry (e.g., oxygen content). Also internal interfaces can arise, e.g., from grain boundaries in ceramic samples or planar crystal defects (e.g., twin boundaries). In general, surface-related effects (SBLCs) represent a problem for technical application as they do not scale down in accord with sample size and especially in the common thin-film techniques employed in integrated electronics, much smaller CDCs, if colossal at all, may arise. One may run into similar problems for grain-boundary or defect-generated IBLCs, at least if the film thickness approaches the spatial dimensions of the regions separated by these types of interfaces (grains or crystallites). Nevertheless, both kinds of IBLCs are used in some types of stand-alone high-capacitance condensers as the mentioned ceramic barrier-layer capacitors and so-called double-layer capacitors (also termed supercapacitors) [100]. The latter can reach capacitances up to several kF making them suitable for energy storage instead of batteries. They use the well-known blocking-electrode effect [18] observed at low frequencies in ionically conducting materials. In contrast to electrons or holes in electronic conductors, ionic charge carriers cannot penetrate into the metallic electrodes used to contact the samples and instead accumulate in thin layers immediately below the sample surface. These insulating and very thin layers represent large capacitors leading, by means of the equivalent circuit

discussed above, to an enhanced capacitance of the sample. For both supercapacitors and ceramic barrier layer capacitors, special preparation techniques are necessary for optimisation of the microstructure. For example in supercapacitors, electrode materials with large inner surfaces like activated charcoal are commonly used.

Of high interest for application may also be any spontaneously arising interfaces caused, e.g., by electronic phase separation or charge order. These phenomena were found in many transition-metal oxides as the colossal magnetoresistance manganites [101,102,103,104] or the cuprate superconductors [105,106,107,108]. Also the system $La_{2-x}Sr_xNiO_4$ attracted much interest due to the formation of stripe-like electronic phase separation in large parts of its phase diagram [109,110,111,112,113,114,115,116,117]. In the charge-ordered or phase-separated phases of many materials, a large or even colossal magnitude of the dielectric constant has been detected (e.g., [38,41,43,51,52,118,119,120,121,122]). The true reason for the found high values of ε' often is not completely clarified but it seems well possible that at least in some cases internal interfaces between the different phase-separated regions may play a role [51,119]. An enhanced dielectric constant due to interfaces between these spontaneously forming heterogeneous regions within the sample still represents a kind of MW effect and no intrinsically large ε' in any parts of the sample has to be assumed to explain the CDC. However, within this scenario the MW relaxation leading to the apparently colossal ε' would arise from an effect that is inherent to the material and does not depend on sample preparation and thus the observed CDCs could be regarded as quasi-intrinsic. In addition, in this case the heterogeneity arises on a much finer scale than, e.g., for contact or grain boundary effects and can be expected to persist also for the scaled down dimensions prevailing in integrated electronics.

2.6 Distinguishing CDCs from interface and intrinsic bulk effects

Distinguishing MW relaxations from intrinsic bulk ones is not a trivial task. As mentioned above, both phenomena can lead to absolutely identical frequency and temperature characteristics of the dielectric quantities. In general, if a strong relaxation mode is observed, with absolute values of ε'_s exceeding 100 and without the typical temperature characteristics of ferroelectrics or relaxor ferroelectrics, a non-intrinsic mechanism is very likely. In such case no exotic mechanisms should be invoked to explain the experimental observations before some additional checks have been performed. Checking for SBLC effects is a relatively simple task. If the formation of Schottky diodes at the electrode-sample interface are suspected, two measurements of the same sample with contacts formed by a conducting paste or paint (e.g., silver paint) and by sputtering or evaporating a metal layer should be performed. Schottky diodes only form if metal and semiconductor are in direct contact. Conducting pastes or paints typically contain metallic grains of μm dimension. It is easy to imagine that these grains "touch" the sample surface only at distinct points and the "wetting" of the sample surface by the metal is poor. Quite in contrast, sputtered or evaporated contacts provide a much better wetting and thus a more effective formation of the thin depletion layer of the Schottky diodes. It should be noted that in case of silver paint at areas, where no direct contact between metal and sample is achieved, the depletion layer of the diode is replaced by air gaps. These gaps of course also act as capacitors, which, however, are of much smaller magnitude due to the larger gap width compared with the thickness of the diode depletion layers and the low $\varepsilon' \approx 1$ of air. (If no Schottky diodes are formed, these air-gap capacitors obviously have too small capacitances to provide any contribution to the measured ε' as, e.g., in $BaTiO_3$ silver paint measurements provide the correct values [11].) Overall, the values of ε_s can be expected to be strongly reduced when using metallic paints or pastes as electrodes. Such a finding clearly points to diode formation at the surface causing the observed CDCs. The thickness of Schottky-diode generated depletion layers depends on the difference of the work functions of metal and semiconductor. Thus at first glance it may seem feasible to simply use two different metals without any further variation of the type of contact. However, the work functions of typical electrode metals do not strongly differ (typically by the order of 10% only) and the effect is barely visible, having in mind that $\varepsilon'(T, \nu)$ often varies by several decades. In contrast, the effect of varying the contact type usually is much bigger and often of the order of one decade or more [11,26,49,51].

Another origin of SBLCs could be deviations from bulk stoichiometry at the surface, e.g., of the oxygen content that may be different to that of the bulk due to the contact with ambient atmosphere. This can lead to the direct generation of a contact capacitance by this layer. Also the formation of a MIS diode with a corresponding thin depletion layer seems possible, with the insulator being the mentioned surface layer of different stoichiometry [25,27,123]. In the latter case, again a variation of contact type should lead to a marked variation of ε_s. In the former case, the same should be achieved by polishing the sample to remove the insulating surface layer and applying the same type of contacts. When doing this, some care should be taken to ensure the same surface roughness before and after polishing as it can be essential for the formation of diodes (see above). Finally, the presence of surface-related effects can also be simply checked for by varying the thickness of the sample [11]. For any kind of SBLC, the sample thickness should directly scale with the absolute value of the CDCs because the surface capacitance remains the same but the geometrical capacitance C_0 used to calculate ε' varies with thickness (see Sec. 2.5). Thus thicker samples should have higher CDC values. Again, when polishing down the sample, the same surface roughness as before must be ensured.

Checking for IBLCs often is a more difficult task. The simplest way to exclude grain boundaries is measuring single-crystalline samples. Alternatively, different grinding of the powders before pressing and sintering and different sintering conditions should be applied to achieve different grain sizes. Insulating grain boundaries may arise from deviations of stoichiometry at the grain surfaces from the bulk one [12] and varying the conditions during preparation may lead to different conductivities, thicknesses etc. of these surface layers. The most commonly applied way to check for grain-boundary effects is the variation of the sintering time applied to the final pressed sample tablets (e.g., [12,20,22]). Usually longer sintering times lead to larger grain sizes. The concomitant reduction of the thickness of the internal barriers, if averaged over the whole sample, leads to an increase of the overall capacitance of the IBLCs. However, one should be aware that longer sintering also should have an effect on the surface of the sample, reducing, e.g., its roughness due to grain growth at the surface. This may also influence possible IBLC formation and makes the interpretation of such experiments somewhat ambiguous. In case of single-crystalline samples, the presence of possible IBLCs caused by twin or other defect-generated boundaries may also be checked by varying the preparation conditions.

Sometimes, instead of presenting the response of CDC materials to ac electric fields via the dielectric constant, loss or conductivity, the complex impedance is provided (e.g., [5,29]). This usually is done by showing complex impedance-plane plots, i.e. $Z''(\nu)$ *vs.* $Z'(\nu)$. In such plots, any parallel RC circuit being part of the equivalent circuit describing the sample (see, e.g., Figs. 1 and 3(c)) will lead to a separate semicircle (at least if their time constants $\tau = RC$ are well separated). As this kind of plots allows for a simple graphical evaluation (e.g., extrapolations of the semicircles enable the determination of the involved resistors of the circuit) they were often employed in earlier times when performing least-square fits of complex functions were a difficult task. However, one has to be aware that the frequency information is lost in this kind of plots and nowadays it is state of the art to perform fits of the dielectric spectra with the complete formula of the equivalent circuit (e.g., Eqs. 1 and 2), simultaneously applied to complemental quantities as, e.g., dielectric constant and conductivity or loss. Sometimes the observation of a second semicircle in the impedance-plane plot, found in addition to the one arising from the bulk, is taken as evidence for grain boundary or other IBLC mechanisms. However, just in the same way as for an IBLC, also an SBLC will lead to such a semicircle and no information concerning the nature of the barrier layers is provided from such type of plots.

Interfacial barrier effects usually lead to relaxation steps in $\varepsilon'(T, \nu)$ with temperature-independent values of ε_s. The static dielectric constant in case of MW relaxations is determined by the interface capacitance C_i (see Sec. 2.5). The thickness of grain boundaries or of depletion layers of diodes usually are not or only weakly temperature dependent, thus explaining the constant $\varepsilon_s(T)$. However, if the interface conductance G_i should be of similar magnitude as the bulk value G_b, i.e. if the condition $G_i \ll G_b$ mentioned in Sec. 2.5 is no longer fulfilled, the relation $C'_s = C_i$ becomes invalid. In this case the low-frequency dielectric constant $\varepsilon_s \propto C'_s$ may become temperature dependent. Assuming $C_i \gg C_b$ and $G_i \approx G_b$ we obtain from Eq. (5):

$$C'_s = \frac{G_b^2 C_i}{(G_i + G_b)^2} \tag{8}$$

The conductivity of bulk and of the barrier layer can be assumed to exhibit strong semiconducting temperature dependence but both quantities usually should not exhibit identical temperature variation and in some temperature region the condition $G_i \ll G_b$ may apply and in others $G_i \approx G_b$ might be valid. Thus, a strong temperature dependence of the static dielectric constant can result due to a transition from $C'_s = C_i$ to C'_s as given by Eq. 8, which, e.g., for $G_i = G_b$ would lead to $C'_s = C_i/4$. Under certain conditions, this can lead to temperature characteristics of ε_s, mimicking that of relaxor ferroelectrics.

3 Colossal dielectric constants: Experimental results

In the following, we provide an overview of results from broadband dielectric spectroscopy on various materials with CDCs as collected in the Augsburg dielectric group during recent years, also including new, so far unpublished data. For details on the dielectric experiments and sample preparation, the reader is referred to our earlier publications, e.g., [11,27,28,29,51,124,125].

3.1 $CaCu_3Ti_4O_{12}$

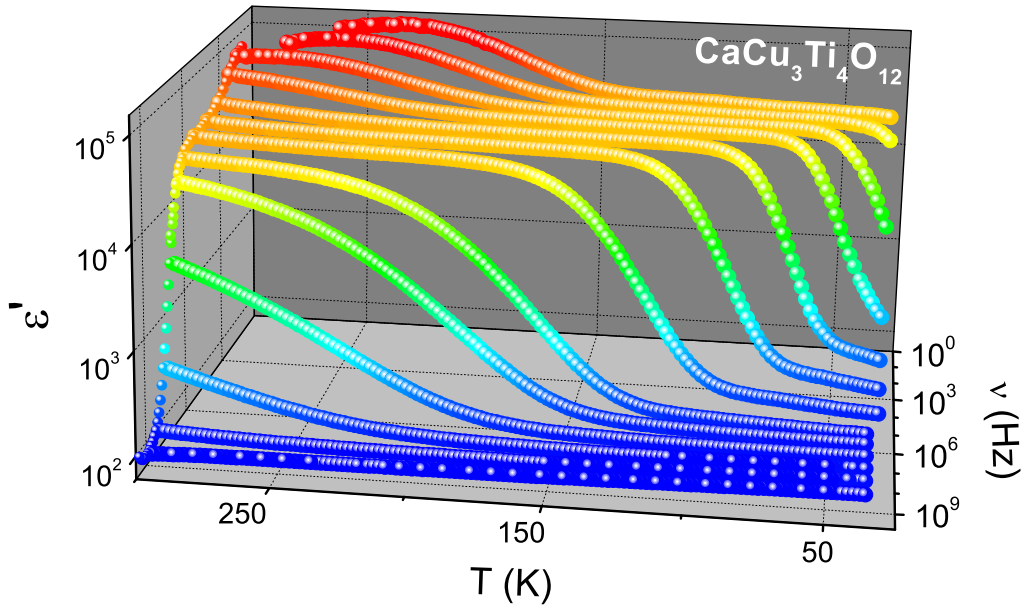

Fig. 4. Temperature- and frequency-dependent dielectric constant of single-crystalline CCTO with silver-paint contacts.

As mentioned above, $CaCu_3Ti_4O_{12}$ is the most prominent material showing CDCs. The three-dimensional representation of Fig. 4 provides a convenient overview of the temperature and frequency dependence of its dielectric constant. Most investigations on CCTO reported in literature were performed on ceramic samples and there were also various efforts to prepare high-quality thin films as a first step to application [126,127,128]. However, the measurements of Fig. 4 were obtained on single-crystalline CCTO, which is only rarely investigated so far [2,26,27]. As pointed out in the original publications [1,2,4], in contrast to ferroelectric materials

the CDC of CCTO remains unchanged in a relatively broad temperature range. In Fig. 4 this region corresponds to the plateau formed by the yellow, orange and red data points. Indeed at the lowest frequencies of the order of several Hz, this plateau extends over the complete temperature range. However, at higher frequencies, this range becomes successively restricted and at frequencies above some 100 MHz no CDCs are observed at all, even at room temperature [11,26]. The reason for this behaviour is the strong relaxational mode typically observed in CCTO. It leads to a step-like decrease of $\varepsilon'(T,\nu)$ with *de*creasing temperature or with *in*creasing frequency. Such characteristics is commonly found also in materials with intrinsic relaxations due to dipolar degrees of freedom [95]. For example, it closely resembles the findings in glass forming liquids with dipolar molecules as, e.g., glycerol, the only difference being the very large values of the static dielectric constant reached at low frequencies and/or high temperatures [129].

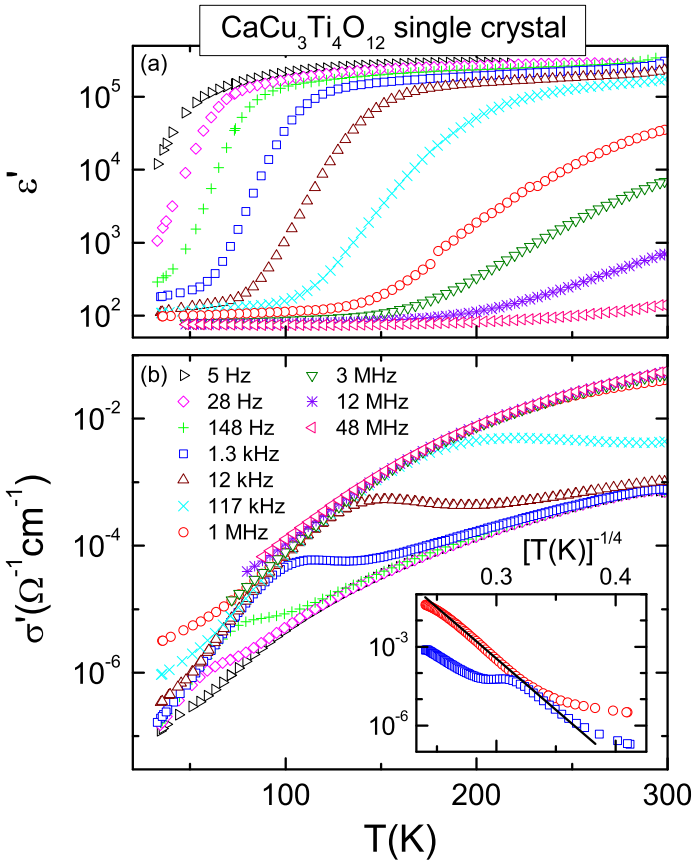

Fig. 5. Temperature-dependent dielectric constant (a) and conductivity (b) of single-crystalline CCTO with sputtered gold contacts at various frequencies [27]. The inset shows the conductivity for 1.3 kHz and 1 MHz in VRH representation. The solid line demonstrates VRH behaviour of the dc conductivity.

In Fig. 5(a) data on the same single crystal, but now using sputtered contacts are provided in a conventional graph showing the temperature dependence of ε' for measurements at different frequencies [27]. The step-like decrease of $\varepsilon'(T)$ with low values at low temperatures arises from a combination of the Debye frequency-dependence shown in Fig. 2 and the semiconductor characteristics of the bulk conductance, which, via $\tau = C_i/G_b$ (see Sec. 2.5), leads to a strong increase of the relaxation time with decreasing temperature. Thus at low temperatures, the system no longer can follow the ac field and low ε' values are observed. In Fig. 5(b) the corresponding conductivity curves are shown. It should be noted that the conductivity is di-

rectly related to the dielectric loss via $\sigma' = \omega\varepsilon''\varepsilon_0$. Thus $\sigma'(T)$ curves are identical to those of $\varepsilon''(T)$, except for their absolute values. However, the additional frequency factor usually leads to a better distinguishability of the different curves and thus to a better readability of the graphs. In addition, in cases of typical interface-generated relaxational response the conductivity representation provides further insight, e.g., concerning the behaviour of the intrinsic bulk conductivity. In general, relaxation steps in ε' should lead to corresponding peaks in ε'' or σ' (for ε'', this is valid for both the temperature and the frequency dependence, cf. Fig. 2). In Fig. 5(b) shoulders are observed instead of peaks because of the additional contribution from the conductance of the interface barrier, which is discussed in more detail below.

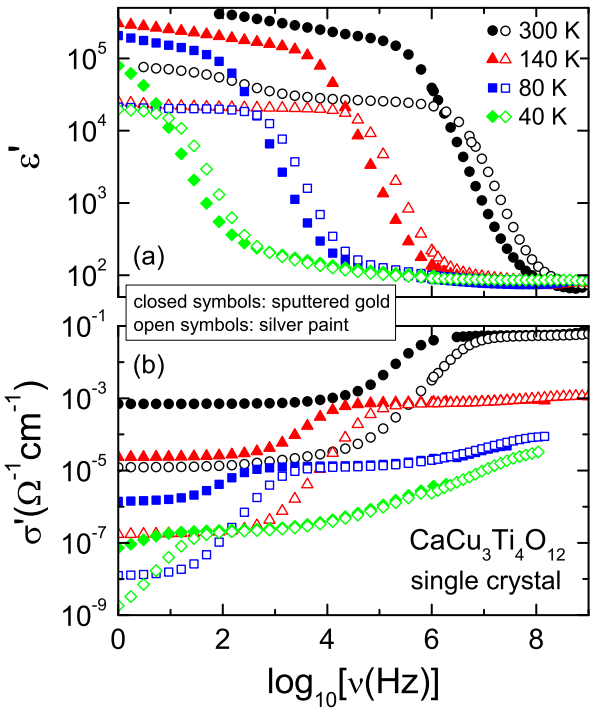

Fig. 6. Frequency-dependent dielectric constant (a) and conductivity (b) of single-crystalline CCTO with silver-paint (open symbols) and sputtered gold contacts (closed symbols) at selected temperatures [27].

In Fig. 6, the frequency dependence of dielectric constant and conductivity are shown for selected temperatures. This figure contains the results from two different measurements using silver paint or sputtered gold contacts applied to the same sample. While at high frequencies the results from both measurements agree, there are marked deviations at lower frequencies. Especially, the static dielectric constant (Fig. 6(a)) reaches values that are about one order of magnitude larger for the sputtered contacts and the low-frequency plateau of $\sigma'(\nu)$ (Fig. 6(b)) even differs by about two decades. These curves are qualitatively similar to the solid lines shown in the schematic plot of Fig. 3 and can be explained in the same way as discussed in detail in Sec. 2.5 in terms of interfacial effects. Within this framework, at low frequencies the response is dominated by the non-intrinsic barrier contribution. Obviously, for sputtered contacts a much higher interfacial capacitance arises. As discussed in detail in Sec. 2.6, this is just what is expected for an SBLC effect caused by the formation of Schottky or MIS diodes at

the electrode-sample interfaces. Also the higher contact conductance of the sputtered contacts, corresponding to the plateau value at low frequencies in $\sigma'(\nu)$, can be understood in this way. It should be noted that even in the sputtered case the contact resistance, while lower than for silver paint, still is considerable and clearly no ohmic contacts are formed. The reason for the different contact conductances obtained for the two contact materials is not the better quality of sputtered contacts. Instead it is due to the variation in the formation of the diodes at the electrodes, which is caused by the different "wetting" as discussed in Sec. 2.6. Obviously, the much higher resistance of the air gaps, replacing parts of the diode depletion layers in the silver-paint case, must play a role here.

According to the equivalent-circuit framework developed in Secs. 2.5 and 2.6, at high frequencies the bulk response should be detected, which is nicely corroborated by the agreement of the curves from both measurements shown in Fig. 6. At 40 K and 80 K, in Fig. 6(b) the bulk conductivity increases with frequency, approaching a power law for the highest frequencies. As discussed in Sec. 2.3, this is the typical UDR arising from hopping of localised charge carriers [76,77,79,80]. The corresponding contribution in $\varepsilon'(\nu)$ is the slight increase with decreasing frequency, best seen in the 40 K curve between about 100 Hz and 100 kHz (cf. dashed line in Fig. 3(a)). Coming now back to Fig. 5(b), the merging of the conductivity curves for different frequencies at low and high temperatures can be understood as follows: The lower merging curve corresponds to the low-frequency plateau seen in the frequency dependence (Fig. 6(b)), i.e. it mirrors the temperature dependence of the contact conductance. The approach of this curve with increasing temperature prevents the observation of well-defined peaks in $\sigma'(T)$, which would become visible only for much smaller contact conductance (see, e.g., Fig. 1 in Ref. [27]). The upper merging curve in Fig. 5(b) corresponds to the intrinsic conductivity of CCTO. At $T < 75$ K deviations arise for the highest frequencies, which signifies just the same UDR contributions as revealed in Fig. 6(b). The intrinsic dc conductivity of CCTO does not follow conventional thermally activated behaviour. Instead it can be quite well described by the prediction of the VRH model [80], i.e. $\sigma_{dc} \propto T^{1/4}$ [27,130,131]. This is demonstrated in the inset of Fig. 5 where the x-axis was chosen to linearise the $T^{1/4}$ law of the VRH model. The curves for 1 MHz and 1.3 kHz, shown in the inset, correspond to the intrinsic dc conductivity for high and low temperatures, respectively. As demonstrated by the solid line, indeed VRH provides a good fit of the data. This is fully consistent with the detection of the typical UDR power law in the frequency dependence, which is characteristic for hopping transport.

The strong dependence of the CDC of CCTO on contact preparation is also found in polycrystals as demonstrated in Fig. 7. Again, strong deviations show up at low frequencies while at high frequencies the bulk response governs the spectra for both types of contact. Taking together all these results, it seems clear that the CDCs in CCTO to a large extent are determined by surface-related effects. However, it should be noted that experiments with varying contacts were reported in literature that partly do not allow for such definite conclusions [14,132,133]. Surface variations introduced by annealing, polishing and other surface treatments obviously also can play an important role, in addition to the effect of the contact material, making the interpretation of experimental results difficult. Finally, it should be noted that for the ceramic sample with sputtered contacts, CDC values of the order of 10^5 are observed (Fig. 7(a)). Usually such high magnitudes of ε' are found for CCTO single crystals only and for polycrystalline samples often much lower values are revealed [1,4,11]. However, annealing the sample for 48h to achieve large grains (see below) and using sputtered contacts to reach good contact wetting obviously can lift the dielectric constant of ceramic samples into similar regions as for single crystals.

As mentioned in Sec. 2.6, sintering of ceramic samples to achieve different grain sizes is a quite commonly employed way of checking for grain-boundary related IBLC effects (e.g., [12,20,22]). Figure 8 shows the frequency-dependent dielectric constant of ceramic CCTO that has been subjected to tempering in air at 1000 °C for 3, 24 and 48 hours [27]. With increasing tempering time, i.e. increasing grain sizes, the magnitude of the CDC increases continuously, while the intrinsic value of ε', read off at high frequencies, remains nearly unaltered. At first glance, this finding seems to strongly point to grain boundaries as the origin of the CDCs as the overall thickness of the interfaces between grains becomes less in relation to the sample thickness

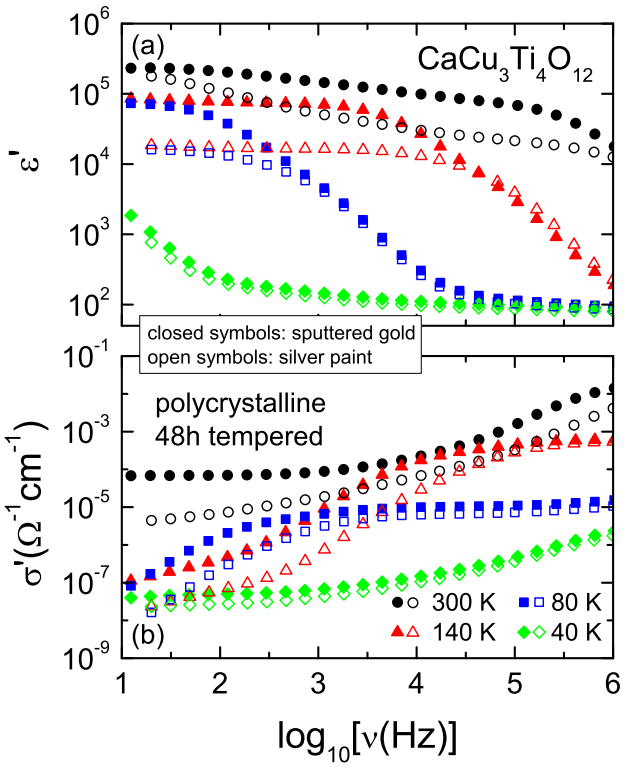

Fig. 7. Frequency-dependent dielectric constant (a) and conductivity (b) of polycrystalline CCTO (48 h tempered) with silver-paint (open symbols) and sputtered gold contacts (closed symbols) at selected temperatures.

and thus the corresponding capacitance increases (see Sec. 2.6). However, as mentioned in Sec. 2.6 also the surface smoothness may change with sintering and therefore an SBLC effect cannot be fully excluded [27]. The effect of sintering on the sample surface is seen in the inset of Fig. 8 providing surface topographies detected by Environmental Scanning Electron Microscopy (ESEM). Indeed for the sample tempered for 48 h, the larger grains also lead to a much smoother surface. In any case, there are several sophisticated experiments reported in literature that seem to suggest that grain boundary or other SBLC mechanisms at least play some role for the generation of the CDCs [9,14,20,23,133]. A solution of the partly contradictory results in literature could be a second relaxation, which was reported in several publications to occur in ceramic samples [11,21,24,26,27] (cf. dotted line in Fig. 3). Thus, one may assume that one relaxation is due to SBLCs and the second one is caused by IBLCs. However, in Ref. [26] it was shown that the second relaxation also shows up in single crystals, excluding a grain boundary mechanism. In fact, this relaxation is also weakly seen in Fig. 6(a) as an additional step-like increase below about 10 kHz revealed by the curve measured at 300 K with silver-paint contacts. It also may well be possible that the domination of the dielectric response by IBLC or SBLC effects is strongly sample dependent and no clear-cut statement for CCTO in general can be made. For example, in Ref. [133] the prevailance of SBLC effects for single crystals and of grain boundary effects for ceramic samples was proposed. Differences may also arise for fine and coarse-grained ceramics or for varying surface resistivities [132].

As revealed by Figs. 5 - 8, the intrinsic dielectric constant of CCTO, which can be read off at high frequencies and/or low temperatures is of the order of 100 and thus relatively

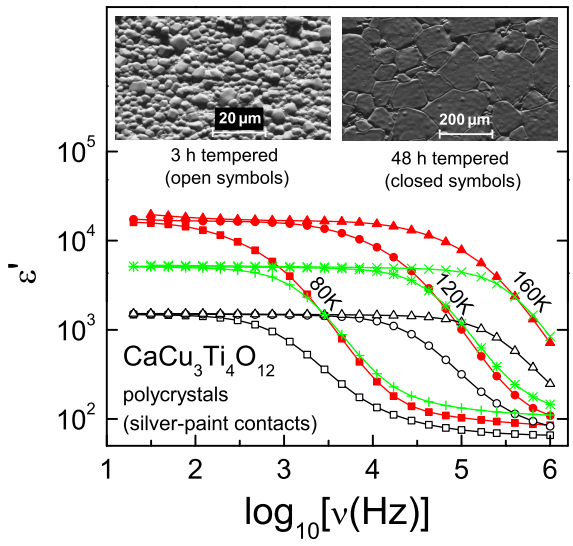

Fig. 8. Frequency-dependent dielectric constant of ceramic CCTO samples tempered for 3 h (open symbols), 24 h (symbols) and 48 h (closed symbols) with silver-paint contacts [27]. The insets show the surface topographies obtained by ESEM of the 3 h and 48 h tempered samples.

high. HfO_2, the most considered high-ε' material for applications in integrated circuits, e.g., has $\varepsilon \approx 22$ only. For heterogeneity-dominated systems, high bulk ε'-values may enhance the CDCs. For example in case of diode-generated SBLCs the capacitance of the depletion layer, which determines the magnitude of the CDC of course depends on the dielectric constant in this region. The depletion layer of course still is CCTO, only depleted from any mobile charge carriers. Its ε', determined by the ionic and electronic polarisability thus should be of similar magnitude at the intrinsic ε' of CCTO. Therefore the CDC should be directly proportional to the bulk value. To understand the generation of the high bulk ε' in CCTO, Fig. 9 shows combined spectra of dielectric, THz and infrared measurements [125]. As revealed by Fig. 9(a), in the narrow frequency region between about 3 and 20 THz, $\varepsilon'(\nu)$ decreases by about one order of magnitude. In this region a number of sharp resonances show up, caused by phononic excitations. Thus, one can conclude that the high intrinsic dielectric constant of CCTO mainly arises from the ionic polarisability. This notion is corroborated by a quantitative evaluation of the phonon modes performed by fitting the spectra using ten oscillators [125]. The resulting sum of the dielectric strengths of all phonon modes is about 77 at room temperature and about 96 at 5 K; the dielectric constant due to electronic polarisability is 6.5. Thus we obtain for the static dielectric constant of the infrared experiment at room temperature $\varepsilon_{s,o} \approx 84$, which agrees well with the intrinsic dielectric constant of the dielectric experiments, $\varepsilon_\infty \approx 83$. With $\varepsilon' \approx 85$ also the result from THz spectroscopy matches these values.

In the combined plot of the conductivity of Fig. 9(b), the sublinear UDR power law arising from hopping conductivity is nicely seen (cf. lower dash-dotted line) but also additional contributions are detected. When also taking into account the THz and infrared results, another steeper power law $\sigma' \propto \nu^n$ with exponent $n \approx 1.4$ shows up (cf. upper dash-dotted line). Indeed, fits assuming the sum of dc conductivity, a sublinear and a superlinear power law (dashed lines) are able to describe the spectra beyond the relaxation mode. It should be noted that via the Kramers-Kronig relation, a superlinear power law in $\sigma'(\nu)$ of course also leads to a contribution in $\varepsilon'(\nu)$, namely an additional decrease proportional to $-\nu^{n-1}$. This decrease is too small to actually show up within the resolution of the experimental data. However, it is observed in the fits shown by the dashed lines in Fig. 9(a) as a slight decrease between 1 GHz and 1 THz. A superlinear power law, showing up at frequencies beyond the validity of the sublinear UDR power

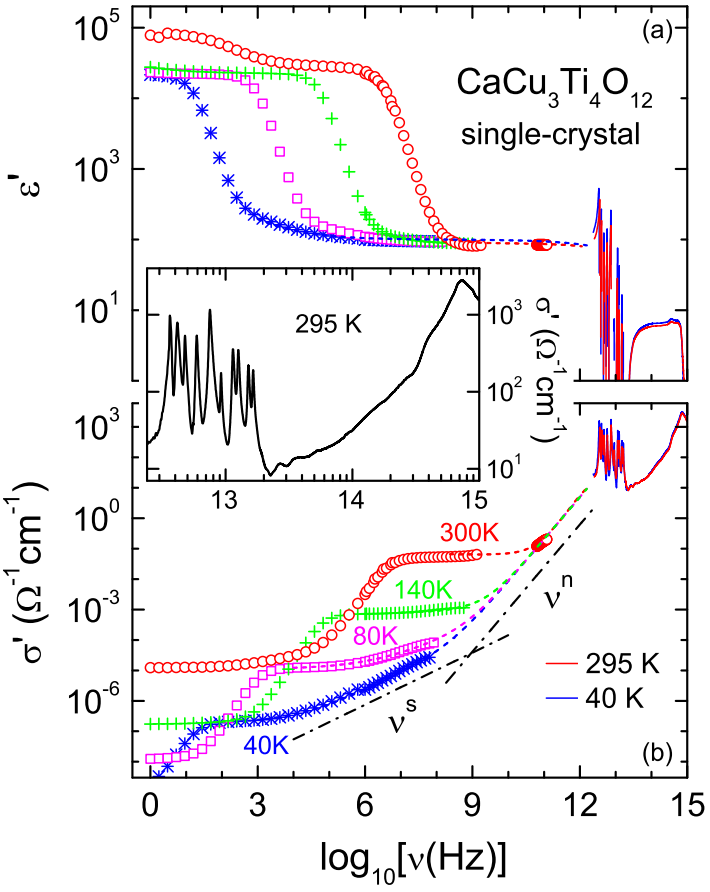

Fig. 9. Dielectric constant (a) and dynamic conductivity (b) of CCTO over 15 decades in frequency for various temperatures [125]. The symbols at $\nu < 10^{12}$ Hz and the lines at $\nu > 10^{12}$ Hz show experimental data. Dashed lines are fits of the data beyond the relaxation, taking into account dc and ac conductivities, the latter described by sub- and superlinear power laws, ν^s and ν^n. The inset shows the dynamic conductivity of CCTO at 295 K in the optical regime.

law, was previously observed in various transition-metal oxides and other materials [48,134]. It is clear that additional contributions beyond the UDR must prevail in the region bridging the gap between dielectric spectroscopy ($\nu \lesssim 1$ GHz) and infrared experiments ($\nu \gtrsim 1$ THz) because in most materials a simple extrapolation of the UDR does not match the absolute values of σ' at the lowest frequencies of the infrared experiments. In Ref. [134] the superlinear ν^n power law was proposed to be a universal property of disordered matter but its microscopic origin still is unclarified. Interestingly, for high frequencies a transition from phonon-assisted to photon-assisted hopping with $\sigma' \propto \nu^2$ is predicted for a Fermi glass [80,135]. However, this transition should appear at $h\nu > k_B T$, which is not fulfilled here.

The inset of Fig. 9 shows a magnified view of the results in the infrared region. At low frequencies, $\nu < 20$ THz, ten phonon modes are clearly revealed. As discussed in detail in Ref. [125], the low-lying modes show a decrease of their eigenfrequencies with decreasing temperature, i.e. their temperature dependence resembles the soft-phonon behaviour that is typical for ferroelectric materials [54]. Thus, while CCTO clearly is not ferroelectric, at least some ferroelectric correlations seem possible, which also is consistent with the increase of the bulk

dielectric constant from 85 at room temperature to about 100 at 5 K revealed by both the dielectric and the infrared experiments [125]. Beyond 20 THz, the further increase of $\sigma'(\nu)$ is due to electronic excitations. They qualitatively agree with the predictions from LSDA band structure calculations [7] assuming transitions from filled hybridised O $2p$ and Cu $3d$ bands to empty O $2p$/Cu $3d$ and Ti $3d$ states [125].

3.2 $CaCu_3Ti_4O_{12}$-related systems

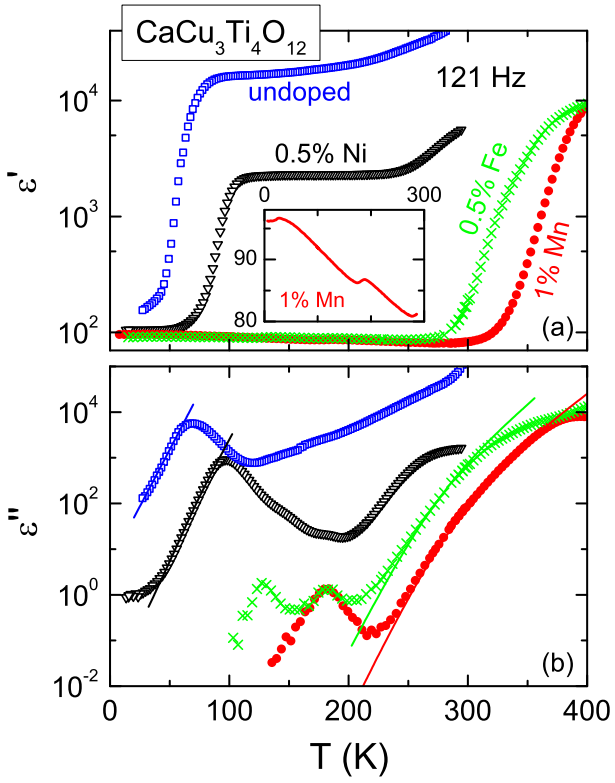

Fig. 10. Temperature-dependent dielectric constant (a) and dielectric loss (b) of undoped and doped (1% Mn, 0.5% Fe and 0.5% Ni) polycrystalline CCTO at 121 Hz [28]. The lines in (b) indicate the temperature-dependent development of the dc conductivity contribution, detected at the low-frequency flank of the MW relaxation peaks. The inset shows a magnified view of $\varepsilon'(\nu)$ for 1% Mn doping below room temperature.

To make use of the CDCs of CCTO for technical applications but avoiding the disadvantages of this materials as, e.g., its relatively high dielectric losses, one can proceed along different routes. Aside of an optimisation of the pure material, for example by adjusting its microstructure, doping of CCTO or the complete substitution with different elements may seem a promising approach. In Fig. 10 we compare the complex permittivity at 121 Hz of pure and three doped CCTO samples [28]. It was previously reported that doping CCTO with Fe or Mn leads to a marked variation of its dielectric constant and a reduction of its dc conductivity [136,137,138,139,140,141]. In Fig. 10(a) the typical MW relaxation step is seen for all investigated materials with CDC values varying between 2000 and 17000. However, for the iron- and

manganese-doped samples, the relaxation step is shifted to much higher temperatures than for the undoped and nickel-doped samples. Quite in general, shifts of relaxational features to higher temperatures correspond to shifts to lower frequencies in frequency-dependent plots and thus (because $\tau \propto 1/\nu_p$ with ν_p the loss-peak frequency) imply an increase of the relaxation times. Obviously, for the Mn- and Fe-doped samples, already shortly below 400 K the relaxation time becomes too large for the systems to follow the excitation frequency of 121 Hz. In contrast, for the pure and Ni-doped sample the relaxation time is much smaller and the materials can follow the frequency for temperatures as low as 100 K before $\varepsilon'(\nu)$ finally relaxes to the intrinsic bulk value of the order of 100.

In Fig. 10(b) the loss peaks corresponding to the MW relaxation are nicely revealed for the undoped and Ni-doped sample. For the Fe- and Mn-doped sample this is not the case and the MW relaxation peak shows up as shoulder at 300-400 K only. There the situation is similar as, e.g., seen in Fig. 5(b) for pure CCTO, which is discussed in detail in Sec. 3.1. As noted above, the marked shift of the MW-relaxation features implies a strong variation of the relaxation time. As $\tau = C_i/G_b$ (see Sec. 2.5), and a variation of C_i is unlikely, the conductivity must be strongly reduced for Fe and Mn doping. This is well corroborated by Fig. 10(b) where the left flanks of the MW-relaxation peaks (indicated by the solid lines) are directly proportional to the dc conductivity (see Sec. 2.5). Obviously, already for relatively small doping levels the dc conductivity becomes reduced by many orders of magnitude when doping CCTO with iron or manganese. Most likely, charge transport in pure CCTO mainly arises from slight oxygen deficiencies, which are compensated by doping with manganese or iron, which should be substituting on the titanium site [28]. In contrast, Ni doping, most likely of isoelectronic type substituted on the copper-place [28], leads to a much smaller reduction of conductivity and thus a smaller shift of the MW relaxation only. These findings demonstrate that reducing the intrinsic bulk conductivity of a material to minimise its dielectric losses is not a suitable approach for its optimisation for technical application in case of a MW-generated mechanism. Reducing the bulk conductance will lead to an increase of the relaxation time and, thus, to a strong restriction of the frequency range available for application. For example, for 1% Mn doping, even at a frequency as low as 121 Hz no CDCs are found anymore at room temperature (Fig. 10(a)). Instead, reducing the conductance of the barrier layers seems to be the more feasible way of optimising MW-dominated CDC materials. This should reduce the losses without affecting the relaxation time. However, a simple increase of the layer thickness will not help as this would lead to a simultaneous reduction of the CDC values.

For the iron- and manganese-doped samples, in Fig. 10(b) two, respectively one additional relaxation peak is revealed at temperatures below the dominating MW loss-peak. Interestingly, the peak located at about 180 K is found for both materials and an evaluation of the frequency-dependent loss reveals that the relaxation time associated with this feature shows identical temperature dependence for both materials [28]. The inset of Fig. 10 demonstrates for the Mn-doped sample that the intrinsic relaxation also shows up in the real part as a small step superimposed to the general decreasing trend of $\varepsilon'(\nu)$. A closer look at the curve for the Ni-doped sample in Fig. 10(b) may also reveal a similar feature for this material. Thus one can suspect that this relaxation is an intrinsic property of CCTO and not related to the doping. It should be noted that for pure CCTO, the intrinsic dielectric properties in this temperature region are inaccessible due to the dominating non-intrinsic barrier contribution (cf. Fig. 5), except for very high frequencies when the MW relaxation is shifted towards high temperatures. However, in this case, also the intrinsic relaxation should be shifted and still may remain undetected. Only the low bulk conductivity of the doped compounds and the subsequent shift of the relaxation feature to higher frequencies could reveal this intrinsic relaxation. Its microscopic origin is unclear at present. The second relaxation in the Fe-doped sample does not show up for Mn doping and thus seems to be related to the Fe defects [137].

As revealed by the inset of Fig. 10, aside of the small relaxation step, the bulk $\varepsilon'(T)$ shows a clear increase with decreasing temperature. This agrees with the findings from measurements at GHz in pure CCTO where the frequency was sufficiently high to shift the MW-relaxation step to temperatures beyond room temperature and also with the results from an analysis of the phonon modes measured by infrared spectroscopy [125]. As discussed above, this finding may

indicate ferroelectric-like correlations in CCTO and there are even speculations about incipient ferroelectricity in doped CCTO [140], similar to $SrTiO_3$ [70]. Another interesting finding is the peak of $\varepsilon'(T)$ occurring just at the transition into an antiferromagnetic state below about 25 K. This small but significant magnetocapacitive effect is discussed in detail in Ref. [28].

Finally, we want to mention the additional increase of $\varepsilon'(T)$ observed at high temperatures, $T \gtrsim 200$ K, in the pure and Ni-doped sample. It signifies the presence of a second relaxation, in addition to the main MW relaxation, which also is of non-intrinsic origin, as briefly discussed above. For a detailed treatment of the second relaxation, see Ref. [27].

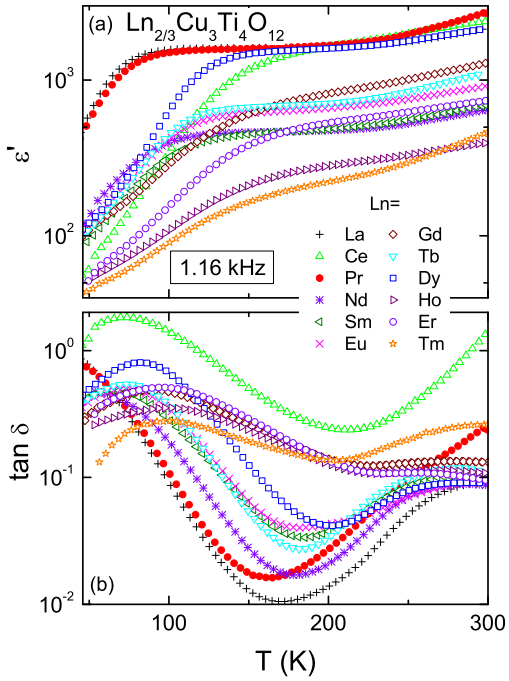

Fig. 11. Temperature-dependent dielectric constant (a) [29] and loss tangent (b) of the investigated LnCTO-compounds at 1.16 kHz (silver-paint contacts).

Already in the pioneering work on CCTO by Subramanian *et al.* and a follow-up paper [1,6], a number of compounds, isostructural to CCTO were introduced. Until now, only few of them are satisfactorily characterised by dielectric spectroscopy and it is not clear why CCTO should be unique within this large group of materials. Indeed, dielectric constants of colossal magnitude were reported for some of these compounds [6,29,30,31,142,143,144,145]. Figure 11 shows the dielectric constant (a) and the loss tangent ($= \varepsilon''/\varepsilon'$) at 1.16 kHz (b) for a number of ceramic $Ln_{2/3}Cu_3Ti_4O_{12}$ samples where Ca was replaced by various lanthanides [29]. In all cases, the typical interface-barrier induced MW relaxation is observed with a high-temperature plateau in $\varepsilon'(T)$ of large magnitude, ε'_s reaching colossal values exceeding 1000 for Ln = La, Ce, Pr and Dy. Among the latter, the cerium compound has the highest loss tangent and seems less suited for application. The relaxation features of the dysprosium compound arise at clearly higher temperatures than for Ln = La and Pr. Thus its relaxation time is higher and the CDC can be expected to occur in a smaller frequency range only (cf. the above discussion of the shift of the relaxations in Fig. 10). $La_{2/3}Cu_3Ti_4O_{12}$ and $Pr_{2/3}Cu_3Ti_4O_{12}$, which behave nearly identical in Fig. 11, seem the most promising materials and in Fig. 12 we provide a more detailed plot of the

dielectric properties of the lanthanum compound. For an in-depth treatment of the dielectric properties of $Pr_{2/3}Cu_3Ti_4O_{12}$, see Ref. [29].

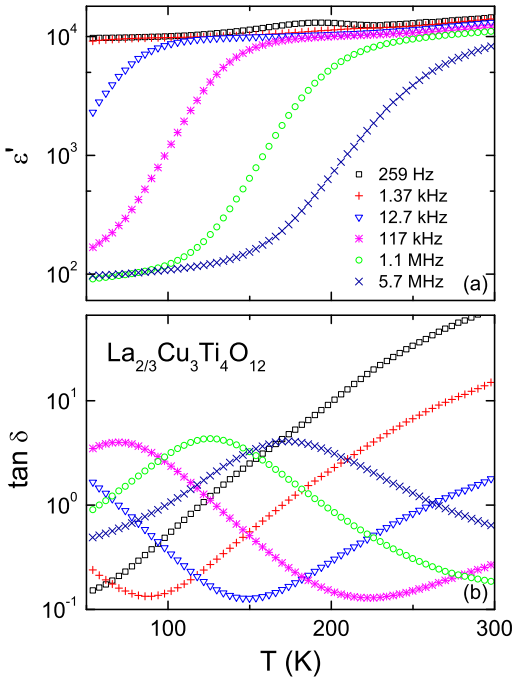

Fig. 12. Temperature-dependent dielectric constant (a) and loss tangent (b) of ceramic $La_{2/3}Cu_3Ti_4O_{12}$ with silver-paint contacts for various frequencies.

Figure 12 shows the temperature dependence of the dielectric constant and loss tangent of $La_{2/3}Cu_3Ti_4O_{12}$ for a number of frequencies. Dielectric properties of this material were also reported in Refs. [30,31,144]. The overall behaviour of $\varepsilon'(T)$ (Fig. 12(a)) closely resembles that of pure CCTO as shown, e.g., in Fig. 5. In contrast to the measurements of $La_{2/3}Cu_3Ti_4O_{12}$, included in Fig. 11, a different sample was used, which was treated to increase the grain size. In this sample, indeed a truly colossal magnitude of ε' of about 10000 is achieved. Interestingly, it seems to arise from an IBLC effect as this value remained nearly unaffected by the type of electrodes used in the measurements (just as for $Pr_{2/3}Cu_3Ti_4O_{12}$; see Ref. [29] for details). The intrinsic ε', read off at low temperatures and high frequencies is about 100, similar as in CCTO. The loss tangent exhibits peaks, which, just as for $\varepsilon''(T)$, are characteristic features of relaxations (see Sec. 2.5). The additional increase at high temperatures arises from the conductance of the barriers, just as the lower merging curve revealed in the conductivity plot of pure CCTO (Fig. 5(b); see also discussion of this figure in Sec. 3.1). Overall, here we have a material that has properties at least as good as CCTO. A similar statement can be made for $Pr_{2/3}Cu_3Ti_4O_{12}$ [29]. Therefore it seems that there is nothing peculiar in CCTO and there may be many more isostructural materials with comparable or even better dielectric properties.

Another promising member of the family of CCTO-related materials is $Cu_2Ta_4O_{12}$. Its crystal structure is derived from that of CCTO by leaving the Ca sites unoccupied and replacing 1/3 of the copper sites by vacancies. Its dielectric behaviour was reported to be similar to that of CCTO, reaching CDCs of about 75000 [49]. For details the reader is referred to Ref. [49].

3.3 $La_{2-x}Sr_xNiO_4$

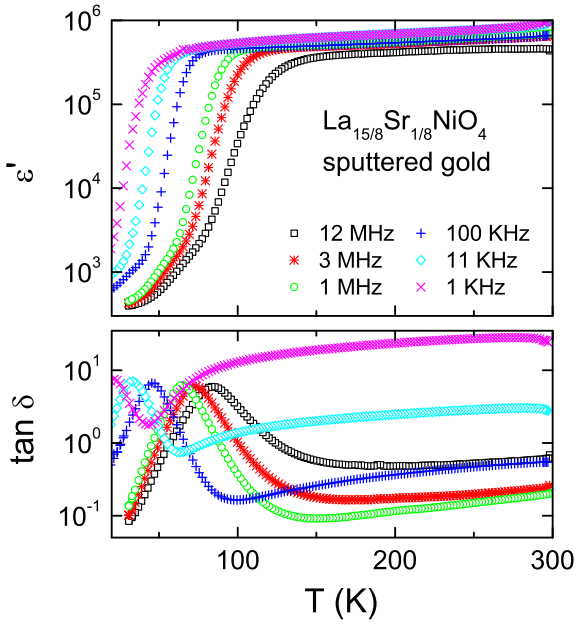

Fig. 13. Temperature-dependent dielectric constant (a) and loss tangent (b) of a LSNO single crystal with sputtered gold contacts for various frequencies [51].

As mentioned in Sec. 2.5, spontaneously arising interfaces caused, e.g., by electronic phase separation or charge order are of high interest for possible applications of CDC materials for capacitive circuit elements. Interestingly there are some reports on CDCs in the system $La_{2-x}Sr_xNiO_4$ [38,41,43], which is known to exhibit electronic phase separation, namely a stripe-like ordering of holes, in large portions of its phase diagram [109,110,111,112,113,114,115,116,117]. In Fig. 13 the temperature dependences of the dielectric constant [51] and the loss tangent of single-crystalline $La_{15/8}Sr_{1/8}NiO_4$ (LSNO) are provided. Typical relaxation steps (a) and peaks (b), just as in CCTO, are revealed with extremely large values of $\varepsilon_s \approx 600000$. The loss tangent at high frequencies is comparable to or even lower than that of CCTO [2].

To elucidate the possible role of SBLCs for the generation of the observed CDCs, in Fig. 14 the frequency dependence of the dielectric constant (a) and the conductivity (b) are provided for both, contacts prepared by sputtering (as in Fig. 13) and by applying silver paint. Just as for CCTO single- and polycrystals (cf. Figs. 6 and 7), a marked variation of ε_s is found with much higher values for the sputtered contacts. Thus, it is clear that surface generated MW effects indeed do contribute to the CDCs in LSNO. Again, at high frequencies the curves obtained with different contact types agree, showing the intrinsic response (for 300 K this regime is reached beyond the investigated frequency range only). The intrinsic $\sigma'(\nu)$ (Fig. 14(b)) is governed by a contribution from dc conductivity (e.g., the approximate plateau at about $2 \times 10^{-4}\ \Omega^{-1}\mathrm{cm}^{-1}$ in the 45 K curves) and a marked UDR power-law increase due to hopping charge transport (see Sec. 2.3). In $\varepsilon'(\nu)$ (Fig. 14(a)), in contrast to CCTO no clear saturation at high frequencies is seen. Obviously, up to the highest frequency the UDR contribution, $\varepsilon' \propto \nu^{s-1}$, is larger than ε_∞ arising from the ionic and electronic polarisabilites. This leads to relatively high values of the intrinsic bulk values of ε' at high frequencies, e.g., $\varepsilon'(1\ \mathrm{GHz}) \approx 300$.

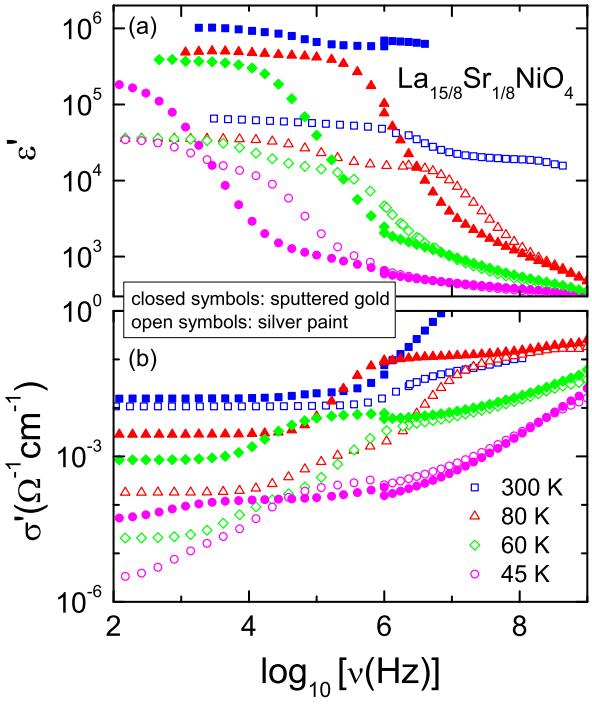

Fig. 14. Frequency-dependent dielectric constant (a) and conductivity (b) of single-crystalline LSNO with silver-paint (open symbols) and sputtered gold contacts (closed symbols) at selected temperatures [51].

The ε' spectra obtained with silver-paint contacts shown in Fig. 14 reveal clear indications for a second relaxation step at low frequencies, quite similar to CCTO [26]. Thus, a further mechanism enhancing ε', in addition to the suspected SBLCs, must be active in this material. In Refs. [51,52] it was speculated that only the second, low-frequency relaxation may be due to an SBLC effect. In the spectra obtained for sputtered contacts, this second relaxation dominates the response and the first, high-frequency relaxation may become undetectable. Then a contribution from the electronic phase separation may well be possible, leading to a distinct separate relaxation step for the silver-paint sample only . Clearly further work is necessary to corroborate this scenario.

In Fig. 15, a combined ε'-spectrum of LSNO is shown for room temperature, including dielectric and infrared data. For comparison also a corresponding spectrum for CCTO is included (same data as in Fig. 9 [125]). This plot reveals a marked difference of the dielectric response of both materials: While $\varepsilon'(\nu)$ of CCTO starts to strongly decrease for frequencies beyond 1 MHz and is far from being colossal at some 100 MHz and in the GHz region, this is not the case for LSNO. Due to the restrictions of the experimental technique employed to cover the MHz to GHz region when measuring very high capacitances, no measurements in LSNO at $\nu > 430$ MHz were possible. However, the dashed line shows the most likely course of $\varepsilon'(\nu)$ beyond this frequency. It is based on an extrapolation of fit parameters from fits at lower temperatures, where the MW-relaxation step is well within the frequency window [51,52]. Overall, LSNO seems to be much better suited than CCTO for applications at frequencies in the MHz-GHz range, which is of high relevance, e.g., in modern telecommunications technology.

Finally, we want to note that the infrared results in LSNO reveal a "static" dielectric constant (which would be denoted as ε_∞ from a dielectric-spectroscopy viewpoint) of approximately

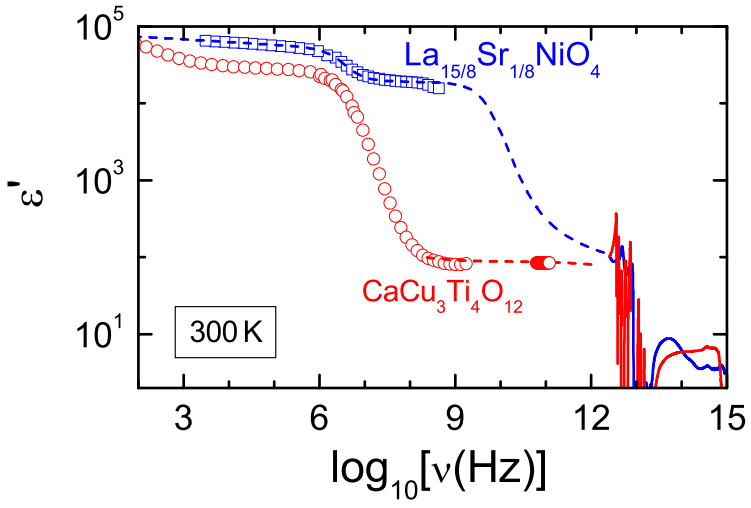

Fig. 15. Comparison of the frequency-dependent dielectric constant of LSNO and CCTO single crystals from dielectric and IR measurements [51,125]. The measurements were performed at room temperature. The upper dashed line was calculated from an extrapolation of the parameters obtained from fits of spectra at lower temperatures (cf. Fig. 2(a) of Ref. [51]). The lower dashed line is a guide to the eyes.

90, much lower than the bulk value of 300 observed at 1 GHz (Fig. 14(a)). This corroborates the above-mentioned scenario of a dominating UDR contribution in $\varepsilon'(\nu)$ up to the highest frequencies covered in the dielectric measurements.

The system $La_{2-x}Sr_xNiO_4$ provides the possibility of tuning the Sr content over a wide range. Figure 16 shows first results demonstrating that, in addition to $x = 1/8$, CDCs are also found for other Sr contents, namely $x = 0.2$ and 0.25 (see also [38,41,43]). In all cases the typical MW relaxation is observed. The approximate agreement of the temperature location of the relaxation steps for the poly- and single-crystalline samples with $x = 1/8$ (cf. Figs. 13 and 16(a)) indicates that also for the ceramic sample the CDC can be expected to persist up to higher frequencies than in CCTO. The same can be said for the compound with $x = 0.2$ while for $x = 0.25$ the relaxation steps seem to be located at somewhat higher temperatures (i.e. the relaxation time is higher). In addition, they are smeared out or even composed of two separate relaxation steps and further investigations are necessary to clarify this issue. In any case it is clear that $La_{2-x}Sr_xNiO_4$ is a promising system that deserves at least as much attention as CCTO and its relatives.

3.4 Other transition-metal oxides with colossal dielectric constants

As mentioned in the introductory section, there are many further transition-metal oxides showing CDCs. Two typical examples are provided in Fig. 17. It shows the frequency dependence of the dielectric constant of single crystalline $La_2CuO_{4+\delta}$, measured at various temperatures. Details have been reported in Refs. [84,146]. In this typical parent compound of high-T_c superconductors, the carrier concentration is rather low ($\delta \sim 0$). Nevertheless, at the bulk-electrode interface a depletion layer is formed and the dielectric constant reaches values of almost 2000 in the audio frequency range even at low temperatures. As we were, at the time of this measurement, only interested in intrinsic properties of $La_2CuO_{4+\delta}$, we focused on low temperatures and high frequencies $\nu > 1$ MHz. At elevated temperatures the contact contribution dominates

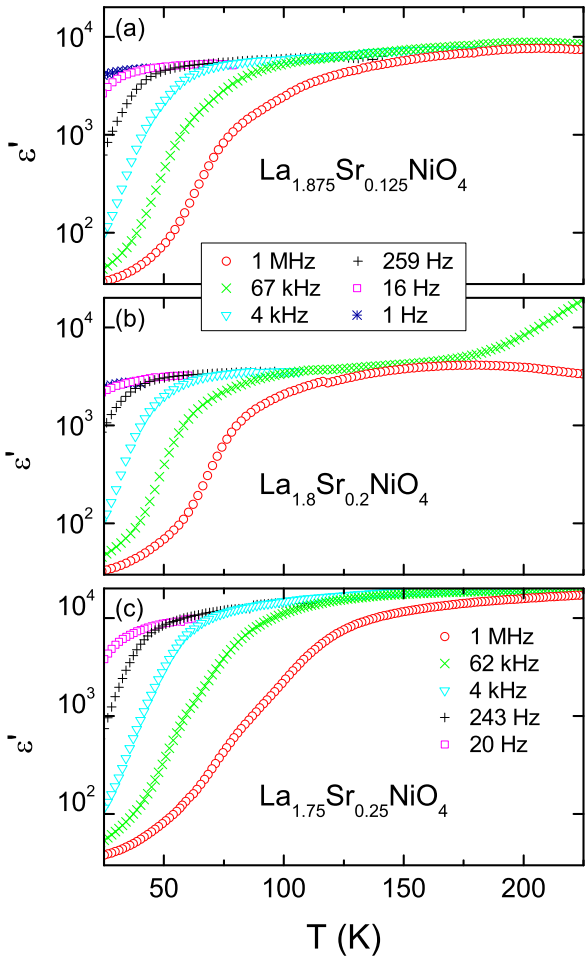

Fig. 16. Temperature dependent dielectric constant of polycrystalline $La_{2-x}Sr_xNiO_4$ samples (tempered for 48 h at 1150 °C, silver-paint contacts) with three different Sr concentrations as measured at various frequencies.

the response far into the microwave regime. The lines in Fig. 17(a) are fits with the equivalent circuit shown in Fig. 3 but without the second interface-related RC element. The intrinsic dielectric constant reaches values of $\varepsilon_\infty \approx 35$.

Figure 17(b) shows results on single-crystalline $Pr_{0.65}Ca_{0.28}Sr_{0.07}MnO_3$ [44], a colossal magnetoresistance material, which is very close to a metal-insulator phase boundary and reveals antiferromagnetism and charge order below about 200 K. Again the solid lines represent fits using the equivalent circuit. The dashed lines indicate the intrinsic response of the sample neglecting contact contributions. The UDR leads to a ω^{s-1} contribution, which smears out the contact-dominated step in $\varepsilon'(\omega)$ at high frequencies. In Pr(Ca : Sr)MnO_3 the intrinsic dielectric constant $\varepsilon_\infty = 50$.

Finally, Fig. 18 provides the dielectric constant of $La_{1.2}Sr_{2.7}IrO_{7.33}$ [50]. This compound is formed by alternative stacking of hexagonal perovskite (A_2IrO_6) and $A'_2O_{1+\delta}$ layers (A = La/Sr; A' = Sr) [147]. In this material, both oxygen and peroxide ions are present, occupying large cavities formed by six AO_6 prisms. Within these cavities, the ions can occupy six different off-centre positions and also the A' ions can assume three different positions within the $A'_2O_{1+\delta}$ layers. Ions in off-centre positions can generate ferroelectricity and also may lead to dipolar relaxation phenomena, which makes this material interesting from a dielectric-spectroscopy viewpoint. In addition, the strong substitutional disorder should give rise to charge-carrier

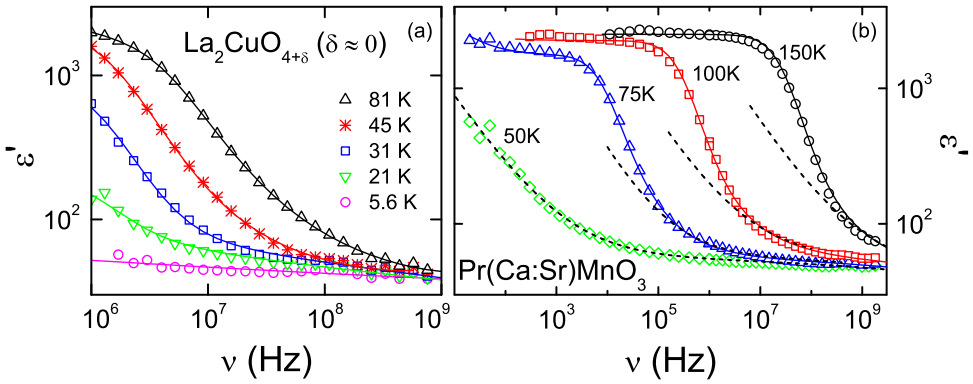

Fig. 17. Spectra of the dielectric constant measured at various temperatures for La_2CuO_4 [84,146] (a) and $Pr_{0.65}Ca_{0.28}Sr_{0.07}MnO_3$ [44] (b). The solid lines are fits with the equivalent circuit shown in Fig. 3 but without the second interface-related RC element. The dashed lines in (b) show the intrinsic response.

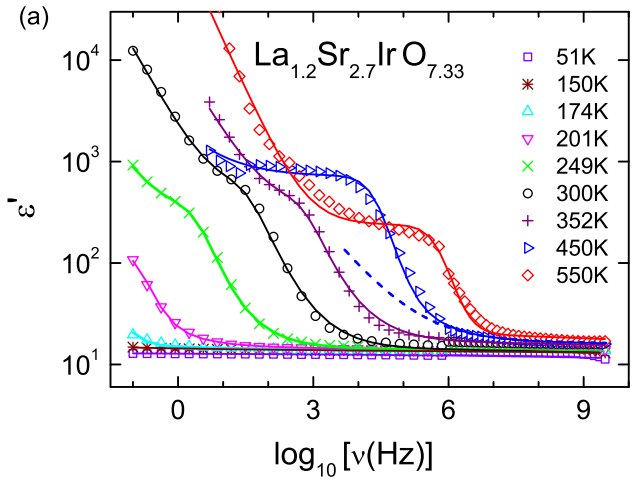

Fig. 18. Spectra of the dielectric constant of $La_{1.2}Sr_{2.7}IrO_{7.33}$ for various temperatures [50]. The solid lines are fits with the equivalent circuit shown in Fig. 3 but without the second interface-related RC element. The dashed line shows the intrinsic response for 450 K.

localisation and the typical signatures of this phenomenon in the ac response. As seen in Fig. 18, for low frequencies $\varepsilon'(\nu)$ reaches the typical plateau of the MW relaxation with CDCs of the order of 1000. However, for further decreasing frequency an additional strong increase shows up. It exhibits no indication of a second plateau as would be expected for a second relaxation feature. Fits of these spectra, which were also simultaneously performed for the conductivity [50], were able to cover this extra increase without assuming a second relaxation (i.e. without a second interfacial RC element, as shown in the equivalent circuit of Fig. 3(c)). A detailed analysis revealed that this low-frequency increase of $\varepsilon'(\nu)$ is due to the strong intrinsic UDR contribution in this material (indicated by the dashed line for 450 K). It is sufficiently strong

to also show up at frequencies below the CDC plateau of the MW relaxation and thus this material provides a nice example for CDCs generated by hopping charge transport (see Sec. 2.3). Measurements with different contact types in this material [50] indicate that the MW relaxation is due to an SLBC mechanism but even without this effect, very large values of ε' would be reached at low frequencies. For a detailed discussion of the dielectric properties of $La_{1.2}Sr_{2.7}IrO_{7.33}$, also revealing an intrinsic dipolar relaxation, see Ref. [50].

4 Summary and Conclusions

A large variety of physical mechanisms can give rise to a colossal magnitude of the dielectric constant. This includes ferroelectricity, with all its disadvantages for technical application, charge-density-wave formation and the approach of a metal-insulator transition, which mostly are of high academic interest only, and interfacial polarisation with its many subgroups as SBLC and IBLC generated effects, including, e.g., electronic phase separation. As revealed by the results provided in the present work, transition-metal oxides in general seem to be prone to the occurrence of colossal magnitudes of the dielectric constant. It is clear that in many cases interfacial barriers within or at the surface of the samples play an important role in the generation of the observed CDCs. Especially in the extensively investigated CCTO, despite some sophisticated attempts of invoking intrinsic mechanisms, a non-intrinsic MW process seems the most likely explanation of its CDCs. However, despite epic efforts of innumerous groups during the past ten years, no consensus on the nature of the involved interfaces has been achieved. In light of the results presented in this work it is clear that in CCTO and also in most other materials, thin insulating layers at the sample surface, most likely induced by diode formation between the metallic electrodes and the semiconducting sample, must play a role. However, also indications for IBLCs of various origins were found. It seems that the question "What causes the CDCs in CCTO?" cannot be unequivocally answered and following the line proposed in Ref. [133] the answer may depend on the specific sample investigated and also combinations of different effects seem likely.

Another outcome of the present work is the finding that CCTO is only one member of a large group of isostructural materials with similar properties, examples being $La_{2/3}Cu_3Ti_4O_{12}$ and $Pr_{2/3}Cu_3Ti_4O_{12}$. Those material show promising dielectric properties and one can expect to discover other, even better suited ones within this vast group of compounds, that indeed once may become new standard materials for high-capacitance applications.

Irrespective of any application viewpoints one should not forget that CCTO and its relatives are highly interesting materials also for purely academic reasons. For example, its relatively high intrinsic dielectric constant, further increasing when lowering the temperature, the softening of several of its phonon modes and the occurrence of isosbestic points in the infrared reflectivity spectra [125] deserves further investigation. It seems likely that ferroelectric correlations are present in CCTO and based on its crystal structure, the Ti^{4+} cation, rattling within the TiO_6 octaeder and tending to go off-centre at low temperatures [1] seems a likely mechanism. Even incipient ferroelectricity may be possible [140].

Among the many other transition-metal oxides with CDCs, the system $La_{2-x}Sr_xNiO_4$ stands out by showing electronic phase separation that may well play an important role in the generation of the observed CDCs in this material. Of special significance is our finding that at room temperature $\varepsilon'(\nu)$ of this material remains colossal well up to the GHz frequency range, quite in contrast to CCTO.

This work was supported by the DFG via the SFB 484 and by the Commission of the European Communities, STREP: NUOTO, NMP3-CT-2006-032644.

References

1. M.A. Subramanian, D. Li, N. Duan, B.A. Reisner, A.W. Sleight, J. Solid State Chem. **151**, 323 (2000)

2. C.C. Homes, T. Vogt, S.M. Shapiro, S. Wakimoto, A.P. Ramirez, Science **293**, 673 (2001)
3. ISI Web of Science, Feb. 2010
4. A.P. Ramirez, M.A. Subramanian, M. Gardel, G. Blumberg, D. Li, T. Vogt, S.M. Shapiro, Solid State Commun. **115**, 217 (2000)
5. D.C. Sinclair, T.B. Adams, F.D. Morrison, A.R. West, Appl. Phys. Lett. **80**, 2153 (2002)
6. M.A. Subramanian, A.W. Sleight, Solid State Sci. **4**, 347 (2002)
7. L. He, J.B. Neaton, M.H. Cohen, D. Vanderbilt, C.C. Homes, Phys. Rev. B **65**, 214112 (2002)
8. M.H. Cohen, J.B. Neaton, L. He, D. Vanderbilt, J. Appl. Phys. **94**, 3299 (2003)
9. S.-Y. Chung, I.-D. Kim, S.-J. L. Kang, Nature Mat. **3**, 774 (2004)
10. P. Lunkenheimer, V. Bobnar, A.V. Pronin, A.I. Ritus, A.A. Volkov, A. Loidl, Phys. Rev. B **66**, 052105 (2002)
11. P. Lunkenheimer, R. Fichtl, S.G. Ebbinghaus, A. Loidl, Phys. Rev. B **70**, 172102 (2004)
12. T.B. Adams, D.C. Sinclair, A.R. West, Adv. Mater. **14**, 1321 (2002)
13. I.P. Raevski, S.A. Prosandeev, A.S. Bogatin, M.A. Malitskaya, L. Jastrabik, J. Appl. Phys. **93**, 4130 (2003)
14. T.B. Adams, D.C. Sinclair, A.R. West, Phys. Rev. B **73**, 094124 (2006)
15. J.C. Maxwell, *A Treatise on Electricity and Magnetism* (Clarendon Press, Oxford, 1873)
16. K.W. Wagner, Arch. Electrotech. **2**, 371 (1914)
17. A.R. Hippel, *Dielectric Materials and Applications* (Artech House, Boston 1954)
18. J. Ross Macdonald, *Impedance Spectroscopy* (John Wiley and Sons, New York, 1987)
19. A.P. Ramirez, G. Lawes, V. Butko, M.A. Subramanian, C.M. Varma, e-print arXiv:cond-mat/0209498
20. B.A. Bender, M.-J. Pan, Mat. Sci. Eng. B **117**, 339 (2005)
21. J.L. Zhang, P. Zheng, C.L. Wang, M.L. Zhao, J.C. Li, J.F. Wang, Appl. Phys. Lett. **87**, 142901 (2005)
22. G. Zang, J. Zhang, P. Zheng, J. Wang, C. Wang, J. Phys. D: Appl. Phys. **38**, 1824 (2005)
23. P. Fiorenza, R. Lo Nigro, C. Bongiorno, V. Raineri, M.C. Ferarrelli, D.C. Sinclair, A.R. West, Appl. Phys. Lett. **92**, 182907 (2008)
24. C.C. Wang, L.W. Zhang, Appl. Phys. Lett. **88**, 042906 (2006)
25. G. Deng, T. Yamada, P. Muralt, Appl. Phys. Lett. **91**, 202903 (2007)
26. S. Krohns, P. Lunkenheimer, S.G. Ebbinghaus, A. Loidl, Appl. Phys. Lett. **91**, 022910 (2007)
27. S. Krohns, P. Lunkenheimer, S.G. Ebbinghaus, A. Loidl, J. Appl. Phys. **103**, 084107 (2008)
28. S. Krohns, J. Lu, P. Lunkenheimer, V. Brize, C. Autret-Lambert, M. Gervais, F. Gervais, F. Bouree, F. Porcher, A. Loidl, Eur. Phys. J. B **72**, 173 (2009)
29. J. Sebald, S. Krohns, P. Lunkenheimer, S.G. Ebbinghaus, S. Riegg, A. Reller, A. Loidl, Solid State Commun. (2010), doi:10.1016/j.ssc.2010.02.006, in press
30. B. Shri Parkash, K.B.R. Varma, Physica B **382**, 312 (2006)
31. B. Shri Parkash, K.B.R. Varma, Physica B **403**, 2246 (2008)
32. G.A. Samara, W.F. Hammetter, E.L. Venturini, Phys. Rev. B **41**, 8974 (1990)
33. C.M. Rey, H. Mathias, L.R. Testardi, S. Skirius, Phys. Rev. B **45**, 10 639 (1992)
34. G.P. Mazzara, S. Skirius, G. Cao, G. Chern, R.J. Clark, J.E. Crow, H. Mathias, J.W. O'Reilly, L.R. Testardi, Phys. Rev. B **47**, 8119 (1993)
35. G. Chern, L.R. Song, J.B. Shi, Physica C **253**, 97 (1995)
36. J.B. Shi, Physica C **305**, 35 (1998)
37. G. Chern, W.K. Hsieh, M.F. Tai, K.S. Hsung, Phys. Rev. B **58**, 1252 (1998)
38. J. Rivas, B. Rivas-Murias, A. Fondado, J. Mira, M.A. Senaris-Rodriguez, Appl. Phys. Lett. **85**, 6224 (2004)
39. N. Biškup, A. de Andrés, J.L. Martinez, C. Perca, Phys. Rev. B **72**, 024115 (2005)
40. J.L. Cohn, M. Peterca, J.J. Neumeier, Phys. Rev. B **70**, 214433 (2004)
41. T. Park, Z. Nussinov, K.R.A. Hazzard, V.A. Sidorov, A.V. Balatsky, J.L. Sarrao, S.-W. Cheong, M.F. Hundley, J.-S. Lee, Q.X. Jia, J.D. Thompson, Phys. Rev. Lett. **94**, 017002 (2005)
42. N. Ikeda, H. Ohsumi, K. Ohwada, K. Ishii, T. Inami, K. Kakurai, Y. Murakami, K. Yoshii, S. Mori, Y. Horibe, H. Kitô, Nature **436**, 1136 (2005)
43. X.Q. Liu, S.Y. Wu, X.M. Chen, H.Y. Zhu, J. Appl. Phys. **104**, 054114 (2008)
44. J. Sichelschmidt, M. Paraskevpoulos, M. Brando, R. Wehn, D. Ivannikov, F. Mayr, K. Pucher, J. Hemberger, A. Pimenov, H.-A. Krug von Nidda, P. Lunkenheimer, V.Yu. Ivanov, A.A. Mukhin, A.M. Balbashov, A. Loidl, Euro. Phys. J. B **20**, 7 (2001)
45. V. Bobnar, P. Lunkenheimer, J. Hemberger, A. Loidl, F. Lichtenberg, J. Mannhart, Phys. Rev. B **65**, 155115 (2002)

46. V. Bobnar, P. Lunkenheimer, M. Paraskevopoulos, A. Loidl, Phys. Rev. B **65**, 184403 (2002)
47. A.I. Ritus, A.V. Pronin, A.A. Volkov, P. Lunkenheimer, A. Loidl, A.S. Shcheulin, A.I. Ryskin, Phys. Rev. B **65**, 165209 (2002)
48. P. Lunkenheimer, T. Rudolf, J. Hemberger, A. Pimenov, S. Tachos, F. Lichtenberg, A. Loidl, Phys. Rev. B **68**, 245108 (2003)
49. B. Renner, P. Lunkenheimer, M. Schetter, A. Loidl, A. Reller, S.G. Ebbinghaus, J. Appl. Phys. **96**, 4400 (2004)
50. P. Lunkenheimer, T. Götzfried, R. Fichtl, S. Weber, T. Rudolf, A. Loidl, A. Reller, S.G. Ebbinghaus, J. Solid State Chem. **179**, 3965 (2006)
51. S. Krohns, P. Lunkenheimer, Ch. Kant, A.V. Pronin, H.B. Brom, A.A. Nugroho, M. Diantoro, A. Loidl, Appl. Phys. Lett. **94**, 122903 (2009)
52. S. Krohns, P. Lunkenheimer, A. Loidl, IOP Conf. Ser.: Mat. Sci. Eng. **8**, 012014 (2010)
53. J. Halblützel, Helv. Phys. Acta. **12**, 489 (1939)
54. M.E. Lines, A.M. Glass, *Principles and applications of ferroelectrics and related materials* (Clarendon Press, Oxford 1979)
55. M. Fujimoto, W.D. Kingery, J. Am. Ceram. Soc. **68**, 169 (1985)
56. C.-F. Yang, Jpn. J. Appl. Phys. **35**, 1806 (1996)
57. A.J. Moulson, J.M. Herbert, *Electroceramics* (Chapman & Hall, London 1990).
58. D. Starešinić, K. Biljaković, P. Lunkenheimer, A. Loidl, Solid State Commun. **137**, 241 (2006)
59. F. Schrettle, P. Lunkenheimer, J. Hemberger, V.Yu. Ivanov, A.A. Mukhin, A.M. Balbashov, A. Loidl, Phys. Rev. Lett. **102**, 207208 (2009)
60. L.E. Cross, Ferroelectrics **76**, 241 (1987)
61. A.A. Bokov, Z.-G. Ye, J. Mat. Sci. **41**, 31 (2006)
62. D. Viehland, S.J. Jang, L.E. Cross, M. Wuttig, J. Appl. Phys. **68**, 2916 (1990)
63. V. Westphal, W. Kleemann, M.D. Glinchuk, Phys. Rev. Lett. **68**, 847 (1992)
64. B.E. Vugmeister, H. Rabitz, Phys. Rev. B **57**, 7581 (1998)
65. T. Portengen, T. Östreich, L.J. Sham, Phys. Rev. B **54**, 17452 (1996)
66. C.D. Batista, Phys. Rev. Lett. **89**, 166403 (2002)
67. A.P. Kampf, M. Sekania, G.I. Japaridze, P. Brune, J. Phys.: Condens. Matter **15**, 5895 (2003)
68. P. Monceau, F.Ya. Nad, S. Brazovskii, Phys. Rev. Lett. **86**, 4080 (2001)
69. K.A. Müller, H. Burkard, Phys. Rev. B **19**, 3593 (1979)
70. R. Viana, P. Lunkenheimer, J. Hemberger, R. Böhmer, A. Loidl, Phys. Rev. B **50**, 601 (1994)
71. J. Dumas, C. Schlenker, J. Marcus, R. Buder, Phys. Rev. Lett. **50**, 757 (1983)
72. G. Grüner, Rev. Mod. Phys. **60**, 1129 (1988)
73. R.M. Fleming, R.J. Cava, L.F. Schneemeyer, E.A. Rietman, R.G. Dunn, Phys. Rev. B **33**, 5450 (1986)
74. R.J. Cava, P. Littlewood, R.M. Fleming, R.G. Dunn, E.A. Rietman, Phys. Rev. B **33**, 2439 (1985)
75. P.B. Littlewood, Phys. Rev. B **36**, 3108 (1987)
76. A.R. Long, Adv. Phys. **31**, 553 (1982)
77. S.R. Elliott, Adv. Phys. **36**, 135 (1987)
78. A.K. Jonscher, Nature **267**, 673 (1977)
79. A.K. Jonscher, *Dielectric Relaxations in Solids* (Chelsea Dielectrics Press, London 1983)
80. N.F. Mott, E.A. Davis, *Electronic Processes in Non-Crystalline Materials* (Clarendon Press, Oxford, 1979)
81. M. Pollak, T.H. Geballe, Phys. Rev. **122**, 1742 (1961)
82. G.E. Pike, Phys. Rev. B **6**, 1572 (1972)
83. P. Lunkenheimer, A. Loidl, C.R. Ottermann, K. Bange, Phys. Rev. B **44**, 5927 (1991)
84. P. Lunkenheimer, M. Resch, A. Loidl, Y. Hidaka, Phys. Rev. Lett. **69**, 498 (1992)
85. A. Seeger, P. Lunkenheimer, J. Hemberger, A.A. Mukhin, V. Yu. Ivanov, A.M. Balbashov, A. Loidl, J. Phys.: Cond. Matter **11**, 3273 (1999)
86. T.G. Castner, Phil. Mag. **42**, 873 (1980)
87. M. Capizzi, G.A. Thomas, F. DeRosa, R.N. Bhatt, T.M. Rice, Phys. Rev. Lett. **44**, 1019 (1980)
88. H.F. Hess, K. Deconde, T.F. Rosenbaum, G.A. Thomas, Phys. Rev. B **25**, 5578 (1982)
89. A. Pimenov, C. Hartinger, A. Loidl, A.A. Mukhin, V.Yu. Ivanov, A.M. Balbashov, Phys. Rev. B **59**, 12419 (1999)
90. B. Kundys, N. Bellido, C. Martin, Ch. Simon, Eur. Phys. J. B **52**, 199 (2006)
91. N.F. Mott, *Metal-Insulator-Transitions* (Taylor & Francis, London, 1990)
92. W.L. McMillan, Phys. Rev. B **24**, 2739 (1981)
93. R.N. Bhatt, Phil. Mag. B **50**, 189 (1984)

94. C. Aebischer, D. Baeriswyl, R.M. Noack, Phys. Rev. Lett. **86**, 468 (2001)
95. F. Kremer, A. Schönhals (Eds.), *Broadband Dielectric Spectroscopy* (Springer, Berlin, 2002)
96. T. Van Dijk, A.J. Burggraaf, Phys. Status Solidi A **63**, 229 (1981)
97. M.J. Verkerk, B.J. Middelhuis, A.J. Burggraaf, Solid State Ionics **6**, 159 (1982)
98. H. Sillescu, J. Non-Cryst. Solids **243**, 81 (1999)
99. M.D. Ediger, Annu. Rev. Phys. Chem. **51**, 99 (2000)
100. P. Simon, Y. Gogotsi, Nature Mat. **7**, 845 (2008)
101. Y. Yamada, O. Hino, S. Nohdo, R. Kanao, T. Inami, S. Katano, Phys. Rev. Lett. **77**, 904 (1996)
102. M. Uehara, S. Mori, C. H. Chen, S.-W. Cheong, Nature **399**, 560 (1999)
103. A. Moreo, S. Yunoki, E. Dagotto, Science **283**, 2034 (1999)
104. E. Dagotto, T. Hotta, A. Moreo, Phys. Rep. **344**, 1 (2001)
105. V.J. Emery, S.A. Kivelson, Physica C **209**, 597 (1993)
106. J.M. Tranquada, B.J. Sternlieb, J.D. Axe, Y. Nakamura, S. Uchida, Nature **375**, 561 (1995)
107. J.M. Tranquada, H. Woo, T.G. Perring, H. Goka, G.D. Gu, G. Xu, M. Fujita, K. Yamada, Nature **429**, 534 (2004)
108. D. Reznik, L. Pintschovius, M. Ito, S. Iikubo, M. Sato, H. Goka, M. Fujita, K. Yamada, G.D. Gu, J.M. Tranquada, Nature **440**, 1170 (2006)
109. C.H. Chen, S.W. Cheong, A.S. Cooper, Phys. Rev. Lett. **71**, 2461 (1993)
110. V. Sachan, D.J. Buttrey, J.M. Tranquada, J.E. Lorenzo, G. Shirane, Phys. Rev. B **51**, 12742 (1995)
111. S.H. Lee, S.W. Cheong, Phys. Rev. Lett. **79**, 2514 (1997)
112. J.M. Tranquada, D.J. Buttrey, V. Sachan, Phys. Rev. B **54**, 12318 (1996)
113. S. Yamanouchi, Y. Taguchi, Y. Tokura, Phys. Rev. Lett. **83**, 5555 (1999)
114. C.H. Du, M.E. Ghazi, Y.Su, I. Pape, P.D. Hatton, S.D. Brown, W.G. Stirling, M.J. Cooper, S.W. Cheong, Phys. Rev. Lett. **84**, 3911 (2000)
115. S.H. Lee, J.M. Tranquada, K. Yamada, D.J. Buttrey, Q. Li, S.W. Cheong, Phys. Rev. Lett. **88**, 126401 (2002)
116. J.M. Tranquada, K. Nakajima, M. Braden, L. Pintschovius, R.J. McQueeney, Phys. Rev. Lett. **88**, 075505 (2002)
117. K. Ishizaka, T. Arima, Y. Murakami, R. Kajimoto, H. Yoshizawa, N. Nagaosa, Y. Tokura, Phys. Rev. Lett. **92**, 196404 (2004)
118. F. Rivadulla, M.A. López-Quintela, L.E. Hueso, C. Jardón, A. Fondado, J. Rivas, M.T. Causa, R.D. Sánchez Solid State Commun. **110**, 179 (1999)
119. S. Mercone, A. Wahl, A. Pautrat, M. Pollet, C. Simon, Phys. Rev. B **69**, 174433 (2004)
120. J. Mira, A. Castro-Couceiro, M. Sánchez-Andújar, B. Rivas-Murias, J. Rivas, M.A. Señaris-Rodríguez, J. Phys. D: Appl. Phys. **39**, 1192 (2006)
121. M. Filippi, B. Kundys, S. Agrestini, W. Prellier, H. Oyanagi, N.L. Saini, J. Appl. Phys. **106**, 104116 (2009)
122. J.L. García-Muñoz, C. Frontera, B. Rivas-Murias, J. Mira, J. Appl. Phys. **105**, 084116 (2009)
123. G. Deng, Z. He, P. Muralt, J. Appl. Phys. **105**, 084106 (2009)
124. U. Schneider, P. Lunkenheimer, A. Pimenov, R. Brand, A. Loidl, Ferroelectrics **249**, 89 (2001)
125. Ch. Kant, T. Rudolf, F. Mayr, S. Krohns, P. Lunkenheimer, S.G. Ebbinghaus, A. Loidl, Phys. Rev. B **77**, 045131 (2008)
126. Y. Lin, Y.B. Chen, T. Garret, S.W. Liu, C.L. Chen, L. Chen, R.P. Bontchev, A. Jacobson, J.C. Jiang, E.I. Meletis, Appl. Phys. Lett. **81**, 631 (2002)
127. R.L. Nigro, R.G. Toro, G. Malandrino, I.L. Fragala, M. Losurdo, M.M. Giangregorio, G. Bruno, V. Raineri, P. Fiorenza, J. Phys. Chem. B **110**, 17460 (2006)
128. P. Fiorenza, R.L. Nigro, A. Sciuto, P. Delugas, V. Raineri, R.G. Toro, M.R. Catalano, G. Malandrino, J. Appl. Phys. **105**, 061634 (2009)
129. P. Lunkenheimer, U. Schneider, R. Brand, A. Loidl, Contemp. Phys. **41**, 15 (2000)
130. L. Zhang, Z.-J. Tang, Phys. Rev. B **70**, 174306 (2004)
131. A. Tselev, C.M. Brooks, S.M. Anlage, H. Zheng, L. Salamanca-Riba, R. Ramesh, M.A. Subramanian, Phys. Rev. B **70**, 144101 (2004)
132. J. Yang, M. Shen, L. Fang, Mat. Lett. **59**, 3990 (2005)
133. M.C. Ferrarelli, D.C. Sinclair, A.R. West, H.A. Dabkowska, A. Dabkowski, G.M. Luke, J. Mat Chem. **19**, 5916 (2009)
134. P. Lunkenheimer, A. Loidl, Phys. Rev. Lett. **91**, 207601 (2003)
135. B.I. Shklovskii, A.L. Efros, Zh. Eksp. Teor. Fiz. **81**, 406 (1981)
136. W. Kobayashi, I. Terasaki, Physica B **329**, 771 (2003)

137. R.K. Grubbs, E.L. Venturini, P.G. Clem, J.J. Richardson, B.A. Tuttle, G.A. Samara, Phys. Rev. B **72**, 104111 (2005)
138. S.-Y. Chung, S.-Y. Choi, T. Yamamoto, Y. Ikuhara, S.-J.L. Kang, Appl. Phys. Lett. **88**, 091917 (2006)
139. M. Li, A. Feteira, D.C. Sinclair, A.R. West, Appl. Phys. Lett. **88**, 232903 (2006)
140. M. Li, A. Feteira, D.C. Sinclair, A.R. West, Appl. Phys. Lett. **91**, 132911 (2007)
141. V. Brize, C. Autret-Lambert, J. Wolfman, M. Gervais, P. Simon, F. Gervais, Solid State Science **11**, 875 (2009)
142. J.J. Liu, C.G. Duan, W.G. Yin, W.N. Mei, R.W. Smith, J.R. Hardy, Phys. Rev. B **70**, 144106 (2004)
143. J.J. Liu, C.G. Duan, W.N. Mei, R.W. Smith, J.R. Hardy, J. Appl. Phys. **98**, 093703 (2005)
144. X.L. Zhou, P.Y. Du, Acta Phys. Sin. **54**, 354 (2005)
145. M.C. Ferrarelli, T.B. Adams, A. Feteira, D.C. Sinclair, A.R. West, Appl. Phys. Lett. **89**, 212904 (2006)
146. P. Lunkenheimer, G. Knebel, A. Pimenov, G.A. Emel'chenko, A. Loidl, Z. Phys. B **99**, 507 (1996)
147. T. Götzfried, A. Reller, S.G. Ebbinghaus, Inorg. Chem. **44**, 6550 (2005)